AGU ADVANCING EARTH AND SPACE SCIENCE

Cretaceous Evolution of the Central Asian Proto-Paratethys Sea: Tectonic, Eustatic, and Climatic Controls

Mustafa Yücel Kaya[1] (ID), Guillaume Dupont-Nivet[1,2,3] (ID), Jean-Noël Proust[2,4] (ID), Pierrick Roperch[2], Niels Meijer[1] (ID), Joost Frieling[5] (ID), Chiara Fioroni[6] (ID), Sevinç Özkan Altiner[7], Marius Stoica[8], Jovid Aminov[9,10], Mehmut Mamtimin[3], and Zhaojie Guo[3]

[1]Institut für Geowissenschaften, Universität Potsdam, Potsdam, Germany, [2]Géosciences Rennes, Université de Rennes, Rennes, France, [3]Key Laboratory of Orogenic Belts and Crustal Evolution, Ministry of Education, Beijing, China, [4]Escuela Politécnica del Litoral (ESPOL), FIMCM-FICT, Guayaquil, Ecuador, [5]Marine Palynology and Paleoceanography, Department of Earth Sciences, Faculty of Geosciences, Utrecht University, Utrecht, Netherlands, [6]Dipartimento di Scienze Chimiche e Geologiche, Via Campi, Università degli Studi di Modena e Reggio Emilia, Modena, Italy, [7]Department of Geological Engineering, Middle East Technical University, Ankara, Turkey, [8]Department of Geology, Faculty of Geology and Geophysics, University of Bucharest, Bucharest, Romania, [9]Institute of Geology, Earthquake Engineering and Seismology, Dushanbe, Tajikistan, [10]Key Laboratory of Continental Collision and Plateau Uplift, Institute of Tibetan Plateau Research, Chinese Academy of Sciences, Beijing, China

Abstract The timing and mechanisms of the Cretaceous sea incursions into Central Asia are still poorly constrained. We provide a new chronostratigraphic framework based on biostratigraphy and magnetostratigraphy together with detailed paleoenvironmental analyses of Cretaceous records of the proto-Paratethys Sea fluctuations in the Tajik and Tarim basins. The Early Cretaceous marine incursion in the western Tajik Basin was followed by major marine incursions during the Cenomanian (ca. 100 Ma) and Santonian (ca. 86 Ma) that reached far into the eastern Tajik and Tarim basins. These marine incursions were separated by a Turonian-Coniacian (ca. 92–86 Ma) regression. Basin-wide tectonic subsidence analyses imply that the Early Cretaceous sea incursion into the Tajik Basin was related to increased Pamir tectonism. We find that thrusting along the northern edge of the Pamir at ca. 130–90 Ma resulted in increased subsidence in a retro-arc basin setting. This tectonic event and coeval eustatic highstand resulted in the maximum observed geographic extent of the sea during the Cenomanian (ca. 100 Ma). The following Turonian-Coniacian (ca. 92–86 Ma) major regression, driven by eustasy, coincides with a sharp slowdown in tectonic subsidence during the late orogenic unloading period with limited thrusting. The Santonian (ca. 86 Ma) major sea incursion was likely controlled by eustasy as evidenced by the coeval fluctuations in the west Siberian Basin. An early Maastrichtian cooling (ca. 71–70 Ma), potentially connected to global Late Cretaceous trends, is inferred from the replacement of mollusk-rich limestones by bryozoan- and echinoderm-rich limestones.

1. Introduction

The proto-Paratethys Sea was a shallow epicontinental sea that extended across Eurasia from the Mediterranean Tethys to China. The proto-Paratethys sea incursions occurred during the Cretaceous and Paleogene until its drastic retreat during the late Eocene, followed by its isolation as the Paratethys during the Oligocene and Miocene (e.g., Kaya et al., 2019; Naidin et al., 1980; Popov et al., 2004). The fluctuations of this sea across Eurasia have not only shaped Asian paleoenvironments but also provide a valuable record of Asian tectonism and eustatism (e.g., Bosboom et al., 2017, 2014; Carrapa et al., 2015; Hendrix et al., 1992; Kaya et al., 2019; Ramstein et al., 1997; Sun et al., 2016; Wang et al., 2019). We focus here on the onset and early history of these fluctuations during the Cretaceous and Early Paleogene because the timing and drivers of the sea incursions into Central Asia still remain unclear. This ambiguity can be attributed to the lack of consensus on the extent, timing, and depositional environments of the sea incursions despite numerous previous studies (e.g., Guo et al., 2015; Hao & Zeng, 1984; Hao et al., 1988; He, 1991; Lan & Wei, 1995; Mao & Norris, 1988; Naidin et al., 1980; Pan, 1991; Pojarkova, 1984; Sobel, 1995; Sun, 1991; Tang, Xue, et al., 1992, 1989; Wang et al., 1990; Wang et al., 2014; Xi et al., 2016; Yang, 1991; Yang et al., 1983, 1995; Zhang, 1992).

These studies propose different interpretations on the age, importance, and even the number of the sea incursions across Central Asia (e.g., Guo, 1991; Hao et al., 1988). These differences may result from the spatially limited observations and from published biostratigraphic ages relatively low in resolution, often based on the benthic fossils carrying significant uncertainty. Recently published reviews of regional geology and radiochronological ages result in contrasting interpretations on the timing of the sea incursions (e.g., Chapman et al., 2019; Xi et al., 2019, and references therein). The lack of higher-resolution age constraints and comprehensive paleogeographic reconstructions implies that the controlling factors for the Cretaceous sea incursions and their potential consequences on Asian environments remain unresolved.

It is often suggested that the Cretaceous transgressions and regressions in the Tajik and Tarim basins were controlled by global sea level fluctuations (Guo et al., 2015; Naidin et al., 1980; Sobel, 1995; Wang et al., 2014; Xi et al., 2016). Yet three prominent geodynamic events, while distant to the south, are usually considered to have governed the Cretaceous subsidence of the Tajik and Tarim basins. As a consequence, it is likely also far-field tectonics influenced the Cretaceous sea incursions. The geodynamic events include (1) the collision of the Lhasa and Qiangtang blocks (e.g., Hendrix et al., 1992; Jolivet, 2017; Sobel, 1999), (2) the collision of the Central Afghan blocks with the southern Eurasian margin (e.g., Montenat, 2009; Tapponnier et al., 1981), and (3) the Kohistan-Ladakh-Eurasia collisions (e.g., Aminov et al., 2017; Bouilhol et al., 2013). These events are important to understand the India-Asia collision, Pamir-Tibetan orogeny, and associated deformation in Central Asia in the form of reactivation of inherited crustal and lithospheric structures (Jolivet, 2017; Robinson, 2015). Better understanding of interactions between these geodynamic mechanisms and basin formation are also required to differentiate tectonic from climatic and eustatic signals recorded in the sedimentary rocks.

The Cretaceous marine record from the Tajik Basin, yet poorly dated and documented, is exceptionally well preserved and exposed, providing an excellent opportunity to assess marine fluctuations and their connections to global climate events. In particular, the early Late Cretaceous period (late Cenomanian-early Turonian, ca. 95–90 Ma) witnessed one of the warmest climates of the past 140 million years followed by a transition to significant global cooling spanning from the late Turonian to the Maastrichtian, ca. 90–66 Ma (Linnert et al., 2014). These multimillion-year global temperature fluctuations in ice-free conditions are generally thought to be driven by a combination of pCO_2 and ocean gateway evolutions (Clarke & Jenkyns, 1999; Friedrich et al., 2012; Linnert et al., 2014; Miller et al., 2005). Short-lived (<1 Ma) Oceanic Anoxic Events (OAEs) associated with episodes of organic carbon burial characterized by the widespread deposition of black shales were also documented in a variety of marine settings under the warm climate of the Aptian-Turonian (ca. 125–90 Ma) (e.g., Schlanger & Jenkyns, 1976). The thick, mollusk- and bryozoa-rich Late Cretaceous carbonate deposits of the Tajik Basin are excellent candidates for the examination of these global climate events. These carbonate-producing organisms react sensitively to changes in the environment (e.g., water depth, light intensity, nutrient input, water temperature, and hydrodynamic energy), and neritic carbonates can hence be used as excellent proxies to reveal environmental changes (e.g., Jaramillo-Vogel et al., 2013; Pomar et al., 2004).

To better understand the timing, cause, and effect of the proto-Paratethys sea fluctuations across Central Asia during Cretaceous time, we studied a suite of sedimentary sections throughout the Tajik and Tarim basins. We analyzed the depositional environments and their evolution to interpret the marine transgressions and regressions and developed an improved regional stratigraphic framework using new biostratigraphic and magnetostratigraphic constraints. The comparison of regional environmental records to established geodynamic/tectonic and global climate events allowed us to discuss the controlling mechanisms behind the sea incursions in the proto-Paratethys sedimentary records.

2. Geological Setting

2.1. Tectonic Setting

The Tajik and Tarim basins are parts of continental fragments successively accreted to each other along a system of sutures mainly related to the Cimmeride and Alpide orogenies (e.g., Robinson, 2015; Şengör, 1984) (Figure 1). The Mesozoic Tajik basin has been interpreted differently as a (1) foreland basin (Chapman et al., 2019; Hamburger et al., 1992; Şengör, 1984), (2) cratonic basin (Burtman, 2000; Burtman & Molnar, 1993; Nikolaev, 2002), (3) passive margin (Leith, 1985), or (4) back-arc basin (Tapponnier
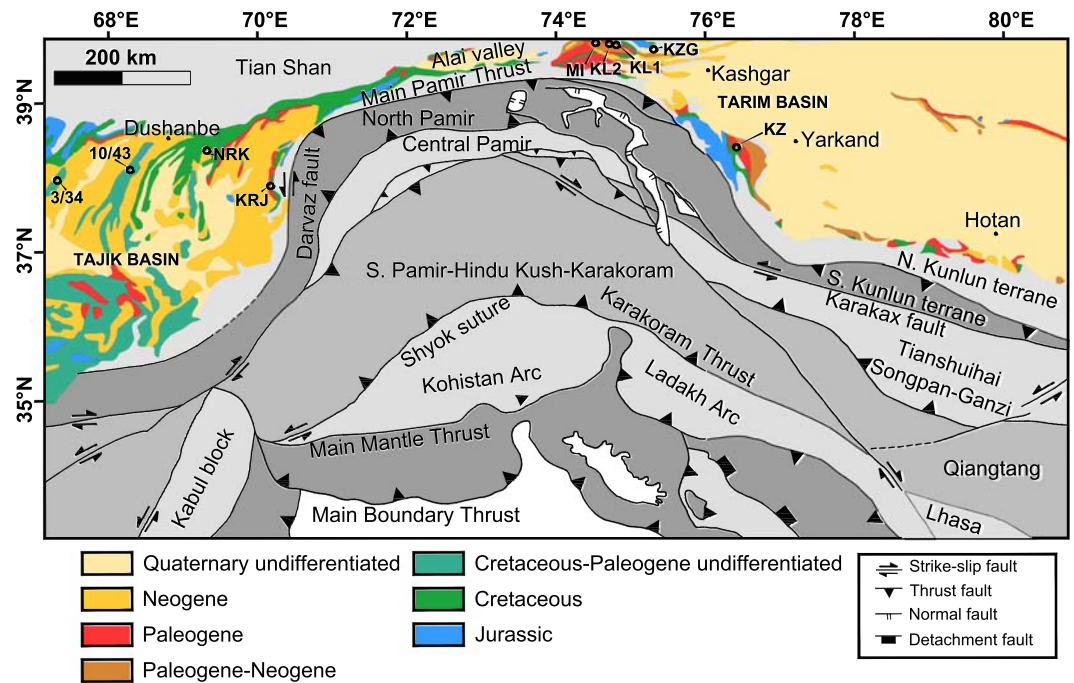
Figure 1. Locations of the studied sections in the Tarim (MI: Mine; KL1: Ka Latale 1; KL2: Ka Latale 2; KZG: Kuzigongsu; KZ: Kezi) and Tajik (NRK: Nurek; KRJ: Khirmanjo) basins on a schematic geologic map with major tectonic domains (shaded in gray) within the Pamir and western Tibetan Plateau in Central Asia (modified from Carrapa et al., 2015, and Cowgill, 2010). Locations of the two sections, 3/34 and 10/43 from Burtman (2000) on which subsidence analysis was performed for the west and central Tajik Basin, are also shown.

et al., 1981; Thomas et al., 1999), whereas the Mesozoic Tarim Basin has been mostly explained as a foreland basin (Hefu, 1986; Hendrix et al., 1992; Watson et al., 1987).

The Pamir separates the Tajik and Tarim basins and forms the western extension of the Tibetan Plateau in an arcuate convex salient (Figure 1). It has generally been divided into three tectonic domains: the North Pamir, Central Pamir, and South Pamir (e.g., Burtman & Molnar, 1993) (Figure 1). The North Pamir is composed of mainly Paleozoic and Triassic (meta)sedimentary and metavolcanic rocks intruded by Triassic-Jurassic granitoids (Schwab et al., 2004). The Central Pamir consists of Paleozoic, Mesozoic (Triassic, Jurassic, and Cretaceous), and Cenozoic (Oligocene) (meta)sedimentary rocks; gneiss domes of various protolith types and ages (He et al., 2019; Schwab et al., 2004); and Late Cretaceous, Eocene, and Miocene igneous rocks (Chapman, Scoggin, et al., 2018). The South Pamir is composed of Paleozoic, Triassic, and Jurassic (meta)sedimentary rocks affected by Cretaceous and Cenozoic magmatism and metamorphism (Schwab et al., 2004). To the south, the Karakoram block consists of deep crustal metamorphics, Cretaceous to Cenozoic intrusive and sedimentary rocks, and the Kohistan-Ladakh block comprises predominantly Cretaceous oceanic island arc rocks (e.g., Blayney et al., 2016). The complex tectonic evolution of the Pamir has been discussed in many studies with several proposed processes such as slab rollback, subduction erosion, subduction accretion, and marginal slab tear (e.g., Burtman & Molnar, 1993; Hamburger et al., 1992; Kufner et al., 2016; Replumaz et al., 2010; Sobel et al., 2013). The formation of the arcuate shape of the Pamir has been interpreted by two end-member models, including the Neogene gradual deformation and the inherited, preexisting arcuate Pamir that was formed by the successive accretions of Paleozoic-Mesozoic continental fragments onto southern Eurasia prior to the India-Asia collision (Blayney et al., 2019; Chen et al., 2018, and references therein).

Before the Paleogene India-Asia collision, several accretionary events might have governed successive regional tectonic regimes, but the timing of these accretionary events and tectonic regime shifts remain poorly constrained. The collision of the Lhasa and Qiangtang blocks, represented by the closure of the Meso-Tethys Ocean, has been controversially dated between middle-late Jurassic and Late Cretaceous (Bian et al., 2017; Kapp et al., 2007; Ma et al., 2017; Sun et al., 2019; Wang et al., 2016; Yang et al., 2019).

Diachronous suturing has also been suggested such that the collision between the Lhasa and Qiangtang blocks appeared earlier in the east during the mid-Jurassic, while initial collision toward the west would have taken place during the late Early Cretaceous to early Late Cretaceous (Guo et al., 2019; Kapp & DeCelles, 2019). To the west, in Afghanistan, a Late Jurassic-Early Cretaceous age has been proposed for the suturing of the Central Afghan blocks to the southern Eurasian margin (e.g., Montenat, 2009; Otto, 1997; Tapponnier et al., 1981). The collision-age between the Kohistan Arc and the southern margin of Eurasia is also highly uncertain and estimates range from 100–80 Ma (Aminov et al., 2017; Borneman et al., 2015; Faisal et al., 2014; Fraser et al., 2001; Robertson & Collins, 2002) to 50–40 Ma (Bouilhol et al., 2013; Khan et al., 2009).

In addition to the commonly accepted Cenozoic thickening that formed the 90 km thick continental crust (Rutte, Ratschbacher, Khan, et al., 2017; Rutte, Ratschbacher, Schneider, et al., 2017; Stübner, Ratschbacher, Rutte, et al., 2013; Stübner, Ratschbacher, Weise, et al., 2013), pre-Cenozoic deformation involving significant Mesozoic upper-crustal shortening and related crustal thickening in the Central and South Pamir has also been proposed (e.g., Aminov et al., 2017; Robinson, 2015). Late Jurassic and mid-Cretaceous crustal shortening and thickening in the North Pamir and Karakoram regions to the north and south of the Central and South Pamir have also been evidenced, suggesting that the Central and South Pamir were similarly affected by the same deformation events (e.g., He et al., 2019; Imrecke et al., 2019; Robinson, 2015; Robinson et al., 2004, 2012).

The evolution of the Tian Shan located north of the Tajik and Tarim basins initiated during the Carboniferous in an ocean subduction-continental accretion complex (Jolivet et al., 2013; Şengör et al., 1993). Limited activity has been reported in the Cretaceous-Early Paleogene before the major exhumation and uplift of the Tian Shan during the Oligocene-Miocene (Sobel et al., 2006; Yang et al., 2015).

2.2. Stratigraphic Setting

Jurassic to Paleogene marine, transitional (mixed terrestrial-marine) and terrestrial sedimentary rocks unconformably overlay the basement in the Tajik Basin. The Jurassic to lower Paleogene rocks, in turn, are unconformably overlain by upper Paleogene-Neogene synorogenic and postorogenic continental clastics. The Mesozoic-Cenozoic strata have been classified and organized in a complex nomenclature of numerous formations (e.g., Brookfield & Hashmat, 2001; Dzhalilov et al., 1982; Nikolaev, 2002). The Tarim Basin Precambrian basement is covered by marine and terrestrial Paleozoic carbonates and fine-grained clastics. The Mesozoic-Cenozoic strata contain terrestrial red clastics and marine carbonates, clastics, and evaporites (e.g., Klocke et al., 2017; Zhang et al., 2013). Cretaceous successions in the western Tarim Basin have been classified into groups of formations defined by their predominantly marine or terrestrial depositional environments. The Lower Cretaceous Kezilesu Group consists of red clastics of conglomerates, sandstones, and mudstones (Guo et al., 2015). The Upper Cretaceous Yingjisha Group is composed of gray marls, mudstones, and carbonates of the Kukebai Formation; red gypsiferous mudstones of the Wuyitake Formation; beige, gray carbonates, and calcareous mudstones of the Yigeziya Formation; and red gypsiferous mudstones of the Tuyiluoke Formation.

We followed mostly the nomenclature used in Dzhalilov et al. (1982) for the stratigraphy of the Tajik Basin. To simplify the stratigraphic classification, we established groups for the local formations in the Tajik Basin based on appropriate geographic names (Table 1). Geographic locations near which the aggregated local formations are present as complete successions were used for naming. The Shirabad-Akkapghigai-Luchak-Derbent-Karakuz-Kaligrek-Okuzbulak-Kizyltash-Almurad Karabil formations were classified together to be the Gashion Group. The Dazgiriak-Talhab-Gazdahana-Tagara-Karikansai-Tjubegatan formations were aggregated into the Baldzhuvon Group, and the Bulgary-Udantu-Daralitau-Sarykamysh-Kattakamysh-Akrabat-Modun formations were aggregated into the Argankun Group. A regional correlation across the Tajik and Tarim basins for the Cretaceous deposits (Table 1) is proposed based on our lithostratigraphic, biostratigraphic, and sequence stratigraphic interpretationspresented in detail later in this paper, along with a review of existing lithostratigraphic descriptions, correlations, and nomenclatures (e.g., Dzhalilov et al., 1982). The Kezilesu Group is correlated to the Gashion Group in the Tajik Basin. The Kukebai Formation is interpreted to be correlative to the Baldzhuvon Group within the Tajik Basin. The Wuyitake and Yigeziya formations are correlated to the Muzrabat Formation and the Argankun Group in the Tajik Basin, respectively.

Table 1
Depositional Ages, Simplified Lithological Descriptions, and Lithostratigraphic Correlations for the Cretaceous Formations and Groups in the Tajik and Tarim Basins

Age	Lithology	Tarim Basin	Tajik Basin		
		This study	Dzhalilov et al. (1982)	Chapman et al. (2019)
		Formation/Group			
Danian-Selandian	Gypsum and dolomites	Aertashi	Akdjar		Bukhara
Maastrichtian-Danian?	Red mudstones with interbeds of red siltstones, sandstones and gypsum	Tuyiluoke			
Santonian - Maastricthian	Limestones, sandy limestones, coquinas, grey and variegated sandstones, marls, mudstones and siltstones bearing bivalves, ammonites, echinoderms with some gypsum interlayers	Yigeziya	Argankun Group	Bulgary Udantu Daralitau Sarykamish Kattakamysh Akrabat Modun	Sangoba / Hasarak-bolo
Late Turonian - Coniacian	Grey mudstones bearing brackish-water ostracods with interbeds of limestones, gypsum, red siltstones and sandstones	Wuyitake	Muzrabat		Hasarak-bolo
Cenomanian - Early Turonian	Grey, dark-grey mudstones bearing ammonites, echinoids and bivalves with interbeds of marls, coquinas, limestones, sandy limestones, sandstones, siltstones and gypsum	Kukebai	Baldzhuvon Group	Dazgiriak Talhab Gazdahana Tagara Karikansai Tjubegatan	Schuchi-poyon
Early Cretaceous	Red terrigenous sandstones and siltstones alternating with claystones, gypsum, dolomites and marls	Kezilesu Group	Gashion Group	Shirabad Akkapghigai Luchak Derbent Karakuz Kaligrek Okuzbulak Kizyltash Almurad Karabil	Schuchi-poyon

Figure 2. Stratigraphic logs of the Nurek, Khirmanjo, Mine, Ka Latale 1, and Ka Latale 2 sections showing biostratigraphic and magnetostratigraphic correlations to the geological time scale (Ogg et al., 2016). The age correlations based on microfossil assemblages are shown by light gray shading corresponding to the stratigraphic ranges of dinoflagellate cysts and nannofossils. FO = first occurrence of important age-diagnostic biomarker species; LO = last occurrence of important age-diagnostic biomarker species. Abbreviations: Ae = Aertashi; Kz = Kezilesu; Tylk = Tuyiluoke; Wy = Wuyitake; Ygz = Yigeziya.

The Tuyiluoke Formation is correlated to the red gypsiferous mudstone unit at the base of the Akdjar Formation in the Tajik Basin. The underlying correlations of the proposed nomenclature are justified in this study.

Table 2
Depositional Ages of the Cretaceous Formations/Groups in the Tarim and Tajik Basins Based on the Fossil Assemblage and Marker Fossils and Their Comparison With Different Studies

Legend: Calcareous nannofossils · Dinoflagellates · Bivalves · Ostracods · Foraminifera

Tajik Basin (Formation/Group)	Tarim Basin	Age	Mao & Norris (1988) (Tarim Basin)	Hao & Zeng (1984) (Tarim Basin)	Hao & Guo (1990) (Tarim Basin)	Yang et al. (1995) (Tarim Basin)	Lan & Wei (1995) (Tarim Basin)	This study (Tarim Basin)	This study (Tajik Basin)	Chapman et al. (2019) (Tajik Basin)
Akdjar	Aertashi	Danian-Selandian			Cibicides sp., Cibicidoides sp., Florilus sp., Anomalina sp., Quinqueloculina sp., Ammobaculites sp., Meloris sp.					
Akdjar	Tuyiluoke	Maastrichtian-Danian								
Argankun Group	Yigeziya	Santonian-Maastrichtian (ca. 86–68? Ma)			Quinqueloculina sp., Triloculina sp., Spiroloculina sp., Massilina sp., Aeronautispirillina sp., Florilus sp., Brizalina sp., Bolivina sp.	Cythereis sp., Bronsteiniana sp., Pontocyprella facilis, Veenia sp., Sarlatina vigeziyaensis, Ovocytheridea sp.	Leptosolen sp., Pholadomyu sp.	Xenascus ceratoides, Florentinia spp., Alterbidinium spp., Spinidinium echinoideum; Fossocytheridea sp., F. aff longicilptica, Xestoleberis sp., Dolocytheridea sp.	Spinidinium echinoideum, Pediastrum sp., Dinogymnium spp., Camnosphaeropsis utinensis, Siderolites cf. calcitrapoides, Praesiderolites dowvillei, P. vidali, Pseudorbitoides sp., Orbitoides sp., Sivasella sp., Lepidorbitoides sp., Historhitoides sp., Planorbulina sp., Vaughanina sp., Nummollotia sp., Planoheterohelix reussi, Muricohedbergella holmdelensis, Sirtina orbitoidiformis, Sulcoperculina sp., Goupillaudina sp., Cibicidoides ? sp., Culcisphaerula innominate; Eiffellithus eximus, Arkangelskiella cymbiformis, Chiastozygus litterarius, Cribrosphaera ehrenbergii, Watznaueria barnesiae, Broinsonia parca constricta, Calculites obscurus, Micula staurophora, Eiffellithus gorkae, Lucianorhabdus cayeuxii, Uniplanarius gothicus, Uniplanarius cf. sissinghi; Veenia donzei, Cythereloidea granulosa, Veeniacythereis begudensis, Imhotepia massoni multipapillata, Paijenborchella (Eopaijenborchella) massoni, Neocythere aff. verbosa, Dolocytheridea (Paracytheridea) sp., Paracypris sp.	Omphalocyclus sp., Lafitteina sp.; Watznaueria barnesiae, Micula staurophora, Lucianorhabdus cayeuxi, Eiffellithus turriseiffellii, Prediscosphaera cretacea, Arkhagelskiella cymbiformis, Broinsonia sp., Eiffellithis eximius, Zeugrhabdotus sp., Staurolites ellipticus, Cretarhabdus surirellus, Cretarhabdus angustiforatus
Muzrabat	Wuyitake	Late Turonian-Coniacian (ca. 92?–86 Ma)	Canningia reticulata zone (middle part of the Wuyitake Fm. and Yigeziya Fm.)		Quinqueloculina sp., Massilina sp., Triloculina sp., Spiroloculina sp., Pararotalia sp., Nonionella sp., Cibicidina sp., Cibicides sp., Nonionellina sp., Heterohelix sp., Hedbergella sp., Guembelitria sp.					
Badzhuvon Group	Kukebai	Cenomanian-Early Turonian (ca. 100–92? Ma)	Alterbidinium emdulatum zone (upper part of the Kukebai Fm.); Cyclonephelium brevispinatum zone (middle/middle part of the Kukebai Fm.)	Migros asiatica, M. spiritensis, M. oryzanus, M. hectori, M. lobatulus, M. guttiformis, Yuania sinjiangensis, Y. sp., Discorbis vescus, D. sp., Nonion sp., Cibicides sp. (upper part of the Kukebai Fm.) Migros asiatica, M. spiritensis, M. oryzanus, M. hectori, M. lobatulus, M. sp. (middle part of the Kukebai Fm.)	Discorbis sp., Nonionella sp., Pullinia sp., Gavelinella sp., Loxoconcha sp., Bythocypris sp., Ammobaculites sp., Hedbergella sp., Guembelitria sp., Heterohelix sp. (upper part of the Kukebai Fm.) Ammobaculites sp., Reophax sp. Ammomarginulina sp. (middle part of the Kukebai Fm.) Discorbis sp., Quinquleoculina sp., Ammobaculites sp., Haploprogonoides sp., Ammotium sp., Ammomarginulina sp. (lower part of the Kukebai Fm.)	Ovocytheridea sp., Pontocyprella sp., Cytherella sp., Schuleridea irinae, Loxoconcha sp., Bythocypris sp., Paracypris cf. princeps (upper part of the Kukebai Fm.) Pontocyprella sp., Cytherella sp. (middle part of the Kukebai Fm.) Ovocytheridea sp., Pontocyprella sp., Cytherella sp. (lower part of the Kukebai Fm.)	Lima marrotiana, Pycnodonte costei, Cyprimeria ? faba (upper part of the Kukebai Fm.) Ostrea vatonmoides, Ostrea oxiana, Lima aff. subrigida (middle part of the Kukebai Fm.) Flaventia ovalis, Ostrea oxiana, Lima aff. subrigida (lower part of the Kukebai Fm.)	Lithosphaeridium siphonophorum, Palaeohystrichophora infusorioides, Apteodinium deflandrei, Oligosphaeridium pulcherrimum, Oligosphaeridium albertense	Palaeohystrichophora infusorioides, P. paleoinfusa, Oligosphaeridium albertense, Alterbidinium spp., Isabelidinium spp., Chatangiella spp., Epiltosphaeridia spinosa, Charentia cuvillieri, Nezzazata simplex, N. sp., Cuneolina pavonia, C. sp., Quinqueloculina sp., Textularia sp., Lenticulian sp., Watznaueria barnesiae, Gartnergo segmentatum, Microrhabdulus decoratus, Rotelapillus biarcus, Eprolithus octoplatus, E. moratus, Quadrum gartneri, Braarudosphaera bigelowii, Cythereis ovata, Cythereloidea hindei, Bairdia aff. pseudoseptentrionalis, Schuleridea aff. jonesiana, Dolocytheridea (Paracytheridea) aff. crassa, Hamocythere harrsiana, Cornicythereis bonnenai, Isocythereis grossauvensis, Neocythere aff. inornata	
Gashion Group	Kezilesu Group	Early Cretaceous								

For the Tajik Basin, a different formation nomenclature has been recently proposed by Chapman et al. (2019) based on their observations and age controls from the Dashtijum section in the southeast Tajik Basin (Table 1). In detail, they defined the Hasarak-bolo, Schuchi-poyon, Sangoba, and Bukhara formations and correlated them with the local formations. The local Dazgiriak-Talhab-Gazdahana-Tagara-Karikansai-Tjubegatan formations are, as described by Dzhalilov et al. (1982), mainly composed of marine strata of gray mudstones, marls with bivalves and ammonites, coquina limestones, and sandstones. These lithologies are very different from the Schuchi-poyon Formation of Chapman et al. (2019) that consists of sandstones, dark red siltstones, and conglomerates interpreted as fluvial channel and overbank deposits. The Hasarak-bolo Formation consists of siltstone and sandstone interpreted as marginal marine deposits (Chapman et al., 2019). Similarly, the Kattakamysh-Akrabat-Modun formations that contain gray mudstones, marls and limestones, and coquina beds (Dzhalilov et al., 1982) are different from the Hasarak-bolo Formation of Chapman et al. (2019). These newly described formations in Chapman et al. (2019) have been interpreted to be time correlative with the local formations of Dzhalilov et al. (1982) mostly based on new age control. The abovementioned lithology differences suggest significant lateral facies change that we have not observed in the field. However, the new age constraints presented here provide facies correlations that are consistent with the nomenclature of Dzhalilov et al. (1982).

3. Materials and Methods

The Nurek (38°21.898′N, 69° 19.997′E) and Khirmanjo (37°54.389′N, 70°9.174′E) sections were analyzed in detail to establish the stratigraphic framework of the Cretaceous sea fluctuations in the Tajik Basin (Figure 1). We also examined five sections (Kuzigongsu 39°44.970′N, 75°17.935′E; Kezi 38°25.078′N, 76°23.229′E; Mine 39°50.860′N, 74°30.124′E; Ka Latale 1 39°49.336′N, 74°41.246′E; and Ka Latale 2 39°50.217′N, 74°39.033′E) from the Tarim Basin (Figure 1). In total, ~4.5 km stratigraphic thickness was measured and logged. Field observations include lithologies, facies, sedimentary structures, fossil content, and discontinuity surfaces. Fine-grained siliciclastic (samples labeled with "B") and carbonate rock samples (labeled with "C") were collected from all sections for biostratigraphic and microfacies analyses. Foraminifera, calcareous nannofossils, ostracods, and dinoflagellate cysts (dinocysts) were identified and used for age correlations based on their previously established age ranges (Figure 2; Table 2; Text S6 for details). In total, 562 carbonate thin sections were analyzed for microfacies analysis, which were used to determine depositional environments. Microfacies analysis in combination with facies descriptions from the field also enabled us to define depositional sequences and their bounding surfaces in a sequence stratigraphic scheme (e.g., Haq et al., 1987). Carbonate grain abundances were estimated using charts of Baccelle and Bosellini (1965). The percentages of components of bryozoa, mollusk, echinoderm, and nonskeletal ooid grains were determined to mechanistically resolve the biotic changes within the Nurek and Khirmanjo sections (Figure 5). We also collected paleomagnetic core samples from the Khirmanjo (82
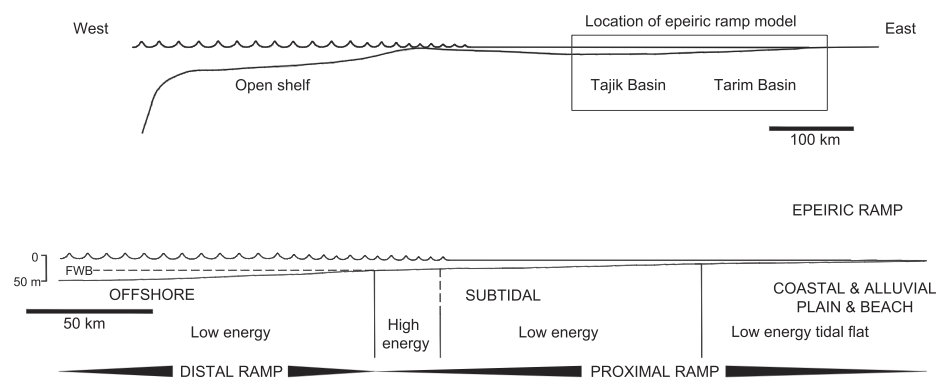
Figure 3. (a) The epeiric ramp model proposed for the Tarim and Tajik Basins (modified from Lukasik et al., 2000). Note that epeiric ramp is located in the east, whereas in the west open shelf conditions prevail. (b) Epeiric ramp model with distal (offshore) and proximal (subtidal, coastal plain, alluvial plain, and occasional beach) parts and their energy conditions. FWB = fair weather wave base.

samples), Mine (60 samples), and Ka Latale 1 (42 samples) sections for magnetostratigraphic analyses. In addition to intrabasinal correlations, interbasinal correlation was conducted by using the sequence stratigraphic interpretations and biostratigraphic constraints from the Nurek, Khirmanjo, Mine, Ka Latale 2, and Ka Latale 1 sections. Details of the sedimentological, sequence stratigraphic, and magnetostratigraphic methods are provided in the supporting information (Texts S1 to S5).

We produced subsidence and relative sea level curves (Figures 6 and S6) based on the results from the sections in the Tajik and Tarim basins to derive implications on the potential controlling mechanisms of the sea incursions. Relative sea level curves were generated by assigning paleo-water depths to the defined facies/microfacies based on their relative positions to each other on the epeiric ramp (Figure 3). Maximum water depth was assumed as 50 and 30 m for distal ramp offshore and proximal ramp subtidal facies, respectively (Lukasik et al., 2000) (Figure S6). Even though there are uncertainties of the assigned paleo-water depth values for the facies/microfacies, their relative position to each other provides solid constraints on the relative sea level change during the Cretaceous sea incursions.

The subsidence curves for the Khirmanjo and Nurek sections in the east Tajik Basin and Kezi and Kuzigongsu sections in the Tarim Basin were produced by performing subsidence analysis using BasinVis 1.0 (Lee et al., 2016). The subsidence analysis integrates the sedimentological, biostratigraphic, and magnetostratigraphic results obtained in this study (see Table S13 for details of the input data for the subsidence analysis). In addition, subsidence analysis for the west and central Tajik Basin was performed on two sections (3/34 and 10/43) from Burtman (2000) (Figure 1). The porosity and compaction coefficients for different lithologies were adopted from Sclater and Christie (1980). Eustatic changes in sea level (Kominz et al., 2008) were included during analysis. The thickness of the red gypsiferous mudstone unit of the Akdjar Formation, correlated to the Tuyiluoke Formation in the Tarim Basin, was taken from Burtman and Molnar (1993). The thickness of the Gashion Group, correlated to the Kezilesu Goup in the Tarim Basin, at the Nurek section was adopted from Leith (1985). The thickness of the Gashion Group at the Khirmanjo section was taken from Burtman and Molnar (1993), whereas that of the Kezilesu Group at the Kuzigongsu and Kezi sections was adopted from Sobel (1995) and Sobel (1999). Subsidence curves display both the total (basement) subsidence and tectonic subsidence calculated by using decompaction and backstripping techniques, respectively.

The local fluctuations in the relative sea level were used along with the subsidence curves to elucidate the potential tectonic and/or eustatic driving mechanisms (Figure 6). Furthermore, the refined age constraints and paleoenvironmental interpretations are combined to generate detailed paleogeographic maps based on the results of this study and existing literature (Figure 8). The maps from the Darius project (Barrier et al., 2018) were updated with data from Kontorovich et al. (2014) for the West Siberian Sea and with data from Kapp and DeCelles (2019) for the Southern Tibet areas.

4. Results and Interpretations

4.1. Biostratigraphy

4.1.1. Calcareous Nannofossils

4.1.1.1. Tajik Basin

4.1.1.1.1. Nurek section

In Sample NR-B25, the presence of *Gartnerago segmentatum* suggests a correlation with the base of the UC2 biozone (Burnett, 1998), early Cenomanian in age (Figure 2).

The assemblage of Sample NR-B27 is characterized by the occurrence of *Microrhabdulus decoratus*, *Rotelapillus biarcus*, and *Eprolithus octopetalus*. The first occurrence of this latter species marks the base of Subzone UC5c, allowing a correlation with the uppermost Cenomanian.

Sample NR-B30 yields few specimens of *M. decoratus*, and very few specimens of *Eprolithus moratus*, suggesting a correlation with the UC6b subzone of the lowermost Turonian. In Sample NR-B35 *E. moratus* is common, indicating an early Turonian age. For Sample NR-B36, a Turonian age is also assigned on the basis of the occurrence of *Quadrum gartneri*, marker of the base of UC7 zone. Based on these results, the Baldzhuvon Group in the Nurek section, which is correlated to the Kukebai Formation in the Tarim Basin, might be Cenomanian to early Turonian in age.

In Sample NR-B44, the occurrence of *Calculites obscurus* yields an age not older than the late Santonian. This species marks the base of zone CC17 (Sissingh, 1977), which has a calibrated age of 84.08 Ma (Gradstein et al., 2012). In the same sample, single specimen of *Uniplanarius* cf. *sissinghi*, marker of the UC15b subzone, could suggest a Campanian age.

4.1.1.1.2. Khirmanjo section

Sample KR-B51 yields very rare specimens of *Calculites obscurus*, *Micula staurophora*, *Eiffellithus gorkae*, *Lucianorhabdus cayeuxii*, and *Uniplanarius gothicus*, indicating an age not older than the late Santonian.

The assemblage of Sample KR-B52 is characterized by the occurrence of very rare specimens of *Eiffellithus eximius* and *Arkangelskiella cymbiformis* and rare specimens of *Chiastozygus litterarius*, *Cribrosphaera ehrenbergii*, *Micula staurophora*, and *W. barnesiae*. The occurrence of *Broinsonia parca constricta*, marker of the base of Subzone UC14b, assigns a Campanian age to this sample.

4.1.2. Dinoflagellates Cyst

4.1.2.1. Tarim Basin

4.1.2.1.1. Mine Section

The lowermost productive samples (MI-B05A and MI-B05B) contain both *Litosphaeridium siphoniphorum* whose last occurrence (LO) was in the Cenomanian-Turonian, ca. 93 Ma (e.g., Pearce et al., 2009), and abundant *Palaeohystrichophora infusorioides* whose first occurrence (FO) was in the Albian-Cenomanian, ca. 100 Ma (e.g., Ogg et al., 2016), suggesting Cenomanian-early Turonian ages. Sample MI-B08 from the Yigeyiza Formation contains a more diverse assemblage, including *Xenascus ceratoides*, diverse *Florentinia* spp., *Alterbidinium* spp., and a few specimens of *Spinidinium echinoideum*. The data constrain the top of the section to an oldest possible age of ca. 87 Ma (late Coniacian) (Lebedeva, 2006; Williams et al., 2004).

4.1.2.1.2. Ka Latale 1 Section

Samples KL1-B01 and KL1-B06 contain abundant *P. infusorioides*, *Oligosphaeridium pulcherrimum*, and *O. albertense* (LO, Cenomanian ca. 95 Ma). However, no species confidently indicate an age older than the Cenomanian. We therefore assign a Cenomanian age to these samples.

4.1.2.1.3. Ka Latale 2 Section

P. infusorioides is very abundant, and the dinocyst assemblages are seemingly similar to those recorded in the Kukebai Formation elsewhere in the Tarim Basin. The presence of *Apteodinium deflandrei* in Sample KL2-B15 suggests an age not older than the Cenomanian. Although few age diagnostic species are present, we note that Turonian or younger marker species appear to be absent.

4.1.2.2. Tajik Basin

4.1.2.2.1. Nurek Section

The productive samples suggest a Cenomanian age for most of the section, with abundant *P. infusorioides* and some *O. albertense*. A more diverse assemblage containing mostly Peridinioid cysts, specifically *Alterbidinium*, *Isabelidinium*, and *Chatangiella*, likely indicates a younger (Turonian) age for the top of the section (Sample NR-B31 and above) (Lebedeva et al., 2013; Williams & Bujak, 1989). The topmost productive sample (NR-B44) yields a few *Spinidinium echinoideum* specimens, and we tentatively assign an age not older than ca. 87 Ma. The presence of *Pediastrum*, a fresh water alga, and abundant plant debris in some samples is noteworthy, as it indicates strong fresh water influence in some intervals.

4.1.2.2.2. Khirmanjo Section

A few diagnostic species were identified, including *P. infusorioides* and *P. paleoinfusa* at the bottom of the analyzed interval (Sample KR-B21). We recorded *Epilosphaeridia spinosa* in Samples KR-B27 and KR-B29, indicating that the lower part of the section has a Cenomanian age. The interval represented by Samples KR-B42 and KR-B43 contains few diagnostic species that are similar to the previously published dinocyst assemblages in Spain (Peyrot, 2011), which may suggest a similar age for the Samples KR-B42 and KR-B43 (Cenomanian-Turonian). The top of the section (Sample KR-B56) is marked by rare occurrences of the genus *Dinogymnium*, which has a first occurrence around or slightly before 90 Ma (Williams et al., 2004). We also recorded a single specimen that can be tentatively assigned to *Cannosphaeropsis utinensis* (FO ca. 85 Ma, top of C34n, late Santonian; Williams et al., 2004) in the same sample.

4.1.3. Foraminifera

4.1.3.1. Tajik Basin

4.1.3.1.1. Nurek Section

The first assemblage from the interval between Samples NR-C41 and NR-C44 contains *Charentia cuvillieri*, *Nezzazatta simplex*, *Cuneolina sp.*, *Quinqueloculina* sp., nodosarids, discorbids, and miliolids. Based on this foraminiferal assemblage, a Cenomanian age has been assigned to this interval (Figure 2).

The second assemblage from the interval between Samples NR-C103 and NR-C110 mainly consists of calcisphaerulids, and very few planktonic foraminifera, such as *Planoheterohelix reussi* and *Muricohedbergella holmdelensis*. Considering the age constraint from the nannofossils analysis of Sample NR-B44 (oldest possible age of late Santonian), coexistence of these species in this interval might suggest a late Santonian-early Campanian age.

The third assemblage at the top of the section, between Samples NR-C120 and NR-C122, is characterized by *Sirtina orbitoidiformis*, *Sulcoperculina* sp., *Goupilloudina* sp., *Cibicidoides*? sp., miliolid forms, and unidentified larger agglutinated forms. This foraminiferal assemblage indicates a Campanian-early Maastrichtian age.

4.1.3.1.2. Khirmanjo Section

Few age diagnostic species, such as *Charentia cuvillieri* and *Cuneolina pavonia*, were recorded in the interval between Samples KR-C36 and KR-C51. Coexistence of these species in this interval suggests a Cenomanian age (Figure 2).

A Turonian-Santonian age might be assigned to the interval between Samples KR-C210 and KR-C228 based on the presence of *Calcisphaerula innominate*; however, a late Santonian age could be assigned more precisely considering the age constraint from the other microfossil analyses (Figure 2).

The third assemblage from the interval represented by Samples KR-C252 and KR-C344 contains larger benthic foraminifera indicating a Santonian-Maastrichtian age. *Praesiderolites douvillei* recorded in Sample KR-C252 suggests a Santonian-Campanian age, whereas the assemblage of *Pseudosiderolites vidali*, *Sirtina orbitoidiformis*, and *Vaughanina* sp. from Sample KR-C299 yields a late Campanian age. The presence of *Pseudosiderolites vidali*, *Sivasella* sp., and *Pseudorbitoides* sp. in Sample KR-C304 suggests Campanian-Maastrichtian boundary interval. An early Maastrichtian age is assigned to Sample KR-C344 based on the presence of *Sirtina orbitoidiformis*, *Siderolites* cf. *calcitrapoides*, and *Lepidorbitoides* sp. (Figure 2).

4.1.4. Ostracods

4.1.4.1. Tajik Basin

4.1.4.1.1. Khirmanjo section

Samples KR-B36, KR-B42, and KR-B46 contain ostracod assemblages indicating a Cenomanian-early Turonian age whereas Sample KR-B49 above contains taxa indicating a Turonian-Maastrichtian age (see Text S6 and Table 2 for the detailed list of ostracod fauna).

4.1.4.2. Tarim Basin

4.1.4.2.1. Mine section

Sample MI-B08 from the base of the Yigeziya Formation contains abundant ostracods with the most common taxon belonging to *Fossocytheridea* sp. aff. *F. longielliptica* indicating a Santonian-Campanian age (Tibert et al., 2003).

4.2. Magnetostratigraphy

4.2.1. Characteristic Remanent Magnetization Directions

Natural Remanent Magnetization (NRM) intensities of the red fine-grained clastics of the Gashion and Kezilesu groups from three sampled sections (Khirmanjo, Mine, and Ka Latale 1) in the Tajik and Tarim basins have mean values of ca. 3 10^{-3} Am^{-1} (Figure S4). The means of the magnetic susceptibility are comparable in the Khirmanjo section in the Tajik Basin (ca. 13 10^{-5} SI) and in the Mine and Ka Latale 1 sections in the Tarim Basin (ca. 8 10^{-5} SI). These relatively low values suggest detrital magnetite is absent in the measured samples. Progressive thermal demagnetization was applied to determine the characteristic remanent magnetization (ChRM). In the Mine and Ka Latale 1 sections, the ChRMs were defined in a temperature range ca. 240–660°C. The vectors were not anchored to the origin because in several samples an ill-defined magnetization was also observed above 660°C. The negative inclination for the in situ direction

of the samples from the Mine section demonstrates that the ChRM is a pretectonic magnetization. In the Tajik Basin, the unblocking temperatures are slightly higher enabling to define ChRMs most likely carried mainly by hematite. The ChRM directions were anchored to the origin. For the Tajik samples, isothermal remanent magnetization (IRM) acquisition and subsequent thermal demagnetization of the IRMs clearly confirm that hematite is the main magnetic carrier in these rocks (Figure S5b). In the Tarim sections, the large unblocking temperature range suggests magnetization mainly carried by pigmentary hematite demagnetized at lower temperatures while the highest unblocking temperatures observed in the Khirmanjo section in the Tajik Basin suggest more detrital hematite. The maximum angular deviation (MAD) values are less than 15° with half of the samples having MAD values less than 5°.

The mean direction for each section was calculated after removing outliers at more than 45° from the mean (Figure S4). After bedding correction, the Khirmanjo section records a significant counterclockwise direction in agreement with the previous results in the Tajik Basin (e.g., Thomas et al., 1994). The low inclination recorded in the Khirmanjo section compared to the one observed in the Ka Latale 1 and Mine sections suggests inclination shallowing due to detrital hematite in the Khirmanjo section while the ChRMs in the Mine and Ka Latale 1 sections are more likely of chemical origin and carried by pigmentary hematite (e.g., Butler, 1992).

4.2.2. Age Correlation

Consistent with our biostratigraphic age constraints, exclusively normal polarities forming a single long normal polarity zone in the Khirmanjo, Mine, and Ka Latale 1 sections indicate deposition within the Cretaceous normal polarity superchron (C34n; ca. 126–84 Ma; Ogg et al., 2016) (Figure 2). However, determination of the upper and lower limits of correlation is not possible.

4.3. Sedimentology and Sequence Stratigraphy Overview

The recognized facies and microfacies were deposited on a ramp composed of alluvial plain, coastal plain-supratidal, intertidal, high-energy shoreface-shoal/beach, low-energy and high-energy subtidal, and off-shore environments (Figure 3; see Text S5 for details). These depositional environments display variable lateral settings and relationships during marine regression and transgression events. The ramp had a width of several hundreds of kilometers extending from the Tarim Basin to the Tajik Basin to the west. With a low bathymetric slope and maximum water depths of tens of meters, it is analogous to the "epeiric ramp" of Lukasik et al. (2000). The epeiric ramp had distal and proximal portions. The offshore-outer ramp facies were deposited in the distal portion, whereas the grain-supported high-energy ramp facies and the low-energy subtidal and tidal flat facies were deposited in the proximal ramp (Figure 3).

The studied interval is divided into six and four depositional sequences (S) in the Tajik and Tarim basins, respectively (Figure 4). Facies/microfacies analyses indicate that the transgressive intervals are represented by offshore, high-energy and low-energy subtidal and intertidal facies bearing distinct fossil assemblages of ostracods, bivalves, gastropods, bryozoa, benthic and planktonic foraminifera, calcareous nannofossils, dinoflagellate cysts, echinoderms, ammonite fragments, and serpulids (see Text S5 for the fossil content of different facies). The regressive intervals are composed of mostly alluvial plain (fluvial and lacustrine) and coastal plain (supratidal) facies including fewer gastropods, bivalves, and some benthic foraminifera or no fossils.

The first sequence (S1) starts with a Lowstand Systems Tract (LST) at the top of the Gashion Group in the Nurek section (Figure 4). This sequence represents the first marine incursion in the eastern Tajik Basin. The first incursion in the Khirmanjo section is based on the presence of marine dinocyst fragments at the base of the section (ca. 30 m). However, due to poor outcrop exposure and lack of high-resolution age constraint, definition of a sequence with its bounding surfaces and its correlation to the Nurek section was arbitrary for this interval in the Khirmanjo section.

An Early Cretaceous sea incursion in the Kangsu area in the Tarim Basin was proposed by Hao et al. (1988) and Guo (1991) based on the presence of marine trace fossils *Ophiomorpha* and *Thalassinoides*, foraminifera *Saccammina globose*, and glauconite abundance data. During fieldwork, we did not find any evidence of this sea incursion in any of our studied sections. Therefore, we argue that, even if this Early Cretaceous sea incursion did occur in the Tarim Basin and might be correlated to the first sea incursion in the eastern Tajik Basin mentioned above, it appears to be absent from our studied sections.
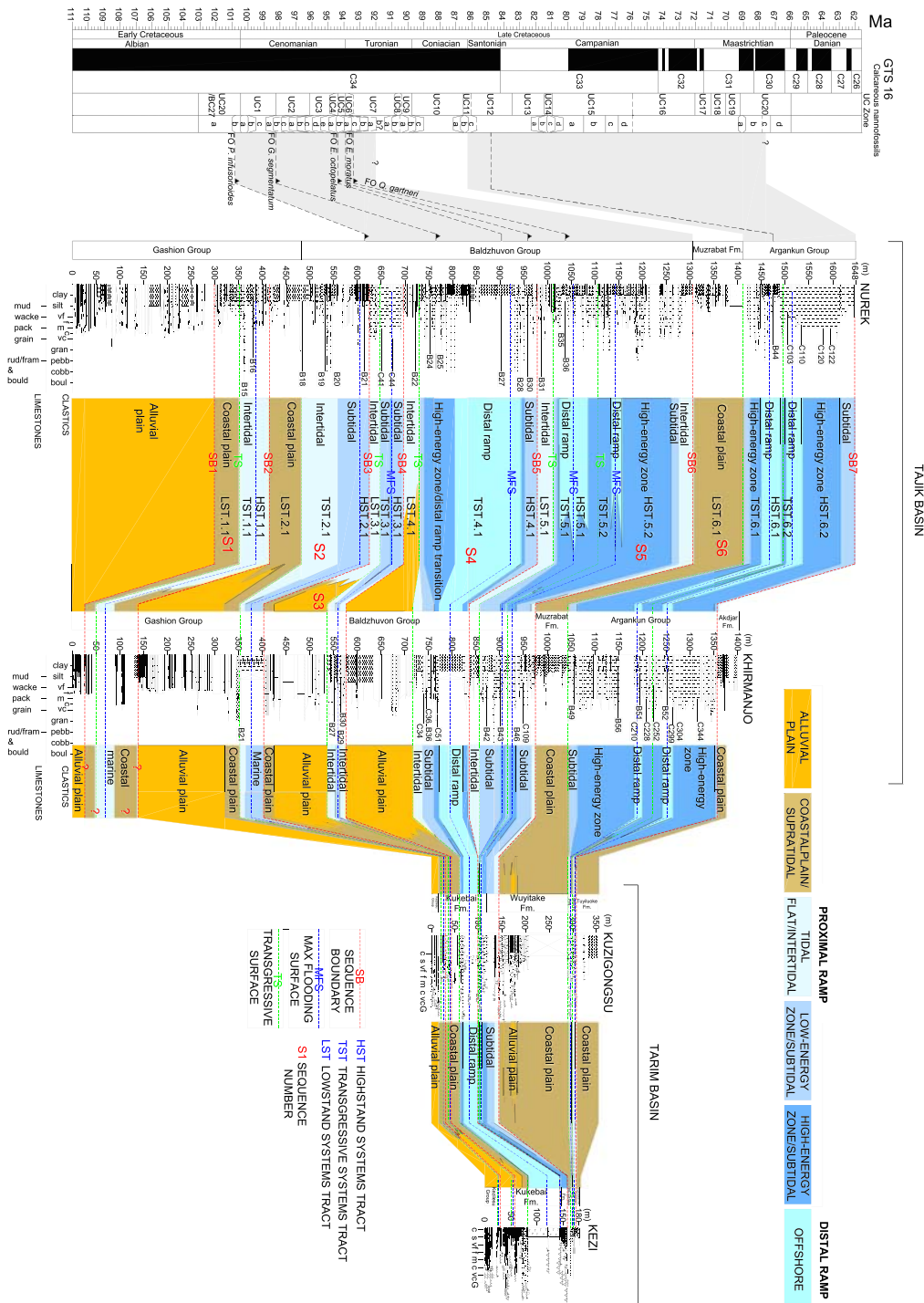
Figure 4. Correlations between the Tajik and Tarim Basins. Stratigraphic logs of the Nurek, Khirmanjo, Kuzigongsu, and Kezi sections are correlated by the sequence stratigraphic relationships and interpretations. Correlation of the identified key bounding surfaces (i.e., sequence boundaries, maximum flooding surfaces, and transgressive surfaces) between the sections enabled us to propose a regional stratigraphic architecture for the Tajik and Tarim basins. Three types of systems tracts have been interpreted; LST, TST, and HST (see legend of the figure the text for the details).

The transgressive surface above the LST of sequence 2 (LST.2.1) represents the second Cretaceous marine incursion during the early Cenomanian with limited geographical extent in the eastern Tajik Basin. This sea incursion did not reach into the Tarim Basin where time-equivalent coastal plain and alluvial plain deposits were found.

The next sequence (S3) presents at the base of the Kukebai Formation and the equivalent Baldzhuvon Group in the Tajik Basin. It starts with the LST.3.1 consisting of alluvial plain and coastal plain deposits in the Khirmanjo, Kuzigongsu, and Kezi sections and intertidal deposits in the Nurek section. S3 represents another Cenomanian marine incursion with limited geographical extent, which, like the early Cenomanian transgression, did not reach the Tarim Basin.

LST.4.1 at the base of the next sequence (S4) is represented with similar depositional environments as in the LST.3.1 in all sections. The transgressive surface at the base of the Transgressive Systems Tract (TST) 4.1 marks the onset of the first major Cretaceous proto-Parathys Sea incursion in Central Asia followed by the buildup of an epeiric mixed siliciclastic-carbonate ramp system in S4 and S5 during the Cenomanian-early Turonian. The proto-Parathys Sea reached its easternmost extent into the Tarim Basin during this sea incursion. The deepest Cretaceous marine environments of the proto-Parathys sea appear in the Transgressive Systems Tracts of sequence 4 (TST.4.1) and sequence 5 (TST.5.1). Remarkably, the marine deposits of the first major sea incursion were not reported from the nearby Dashtijum section (Chapman et al., 2019) despite their occurrence in the Khirmanjo section (this study) and elsewhere in the Tajik Basin (e.g., Naidin et al., 1980; Pojarkova, 1984).

The following sequence (S6) starts with an extended coastal plain deposition during the late Turonian-Coniacian in LST.6.1. This coastal plain deposition was recorded both in the Tajik and Tarim basins representing a major regression in Central Asia. The transgressive surface at the base of the TST.6.1 marks the second major Cretaceous sea incursion during the Santonian, displaying a shift to a carbonate-dominated system on the epeiric ramp both in the Tarim and Tajik basins. S6 ends with shallowing in a Highstand Systems Tract (HST.6.2) and then transition into coastal plain deposition in the following sequence during the Maastrichtian.

4.4. Facies Evolution Based on Predominant Biota

The Late Cretaceous succession in the Nurek and Khirmanjo sections shows a pronounced evolutionary trend (Figure 5). The majority of the fossil-bearing carbonate rocks in the Nurek and Khirmanjo sections are dominated by mollusks (bivalves and gastropods) and small benthic foraminifera, that is, foramol grain association type of Lees and Buller (1972) or molechfor grain association type of Carannante et al. (1988) (Figure 5). Echinoderm-, bryozoa-, and calcisphaerulid-rich or reefal (coral, rudists, and red algae bearing) carbonate lithofacies are also present but less frequent (Figure S3). Lithofacies containing primarily mollusks and benthic foraminifera are abruptly replaced by bryozoan-dominated limestones that contain bryomol grain association type of Nelson (1988) at ca. 1,260 m in the Khirmanjo section and by echinoderm-rich limestones at ca. 1,560 m in the Nurek section (Figure 5). The proportion of echinoderm and bryozoan bioclasts rapidly increases up to ca. 60% and dominates the carbonate lithofacies in the Nurek and Khirmanjo sections, respectively. At the top of the Khirmanjo section, ca. 1,325 m, there is a shift from heterozoan bryozoa-rich to photozoan reefal biota bearing corals, rudists, and red algae.

4.5. Age Control Overview
4.5.1.1.1. Kezilesu and Gashion Groups: Early Cretaceous
The ages of the Kezilesu Group in the Tarim Basin and the correlated Gashion Group in the Tajik Basin (Table 1) were poorly constrained to the Early Cretaceous (ca. 145–100 Ma), mainly relying on lithostratigraphic correlations and relative age determinations (e.g., Baratov et al., 1976). Our magnetostratigraphic results indicate that the deposition of some part of the Kezilesu Group clastics and its Tajik Basin equivalent, Gashion Group, is younger than the base of C34n at circa 126 Ma (Ogg et al., 2016) and older than ca. 100 Ma based on the biostratigraphic constraint of the overlying marine strata (see next paragraph). Recently, Chapman et al. (2019) interpreted the maximum depositional age of the Schuchi-poyon Formation (including the Gashion Group and the base of the overlying Baldzhuvon Group; see Table 1) as 99 ± 6 Ma based on the detrital Zircon Fission Track (ZFT) data from the base of the Dashtijum section, only 15 km north of the Khirmanjo section. Compared to the ca. 100 Ma age of the overlying Baldzhuvon Group, this ZFT age is within error.

4.5.1.1.2. First Major Sea Incursion in the Kukebai Formation-Baldzhuvon Group: Cenomanian-early Turonian (ca. 100–92? Ma)
The age of the Kukebai Formation, correlated to the Baldzhuvon Group in the Tajik Basin, representing the first major transgression extended into the Tarim Basin, is determined to be Cenomanian-early Turonian
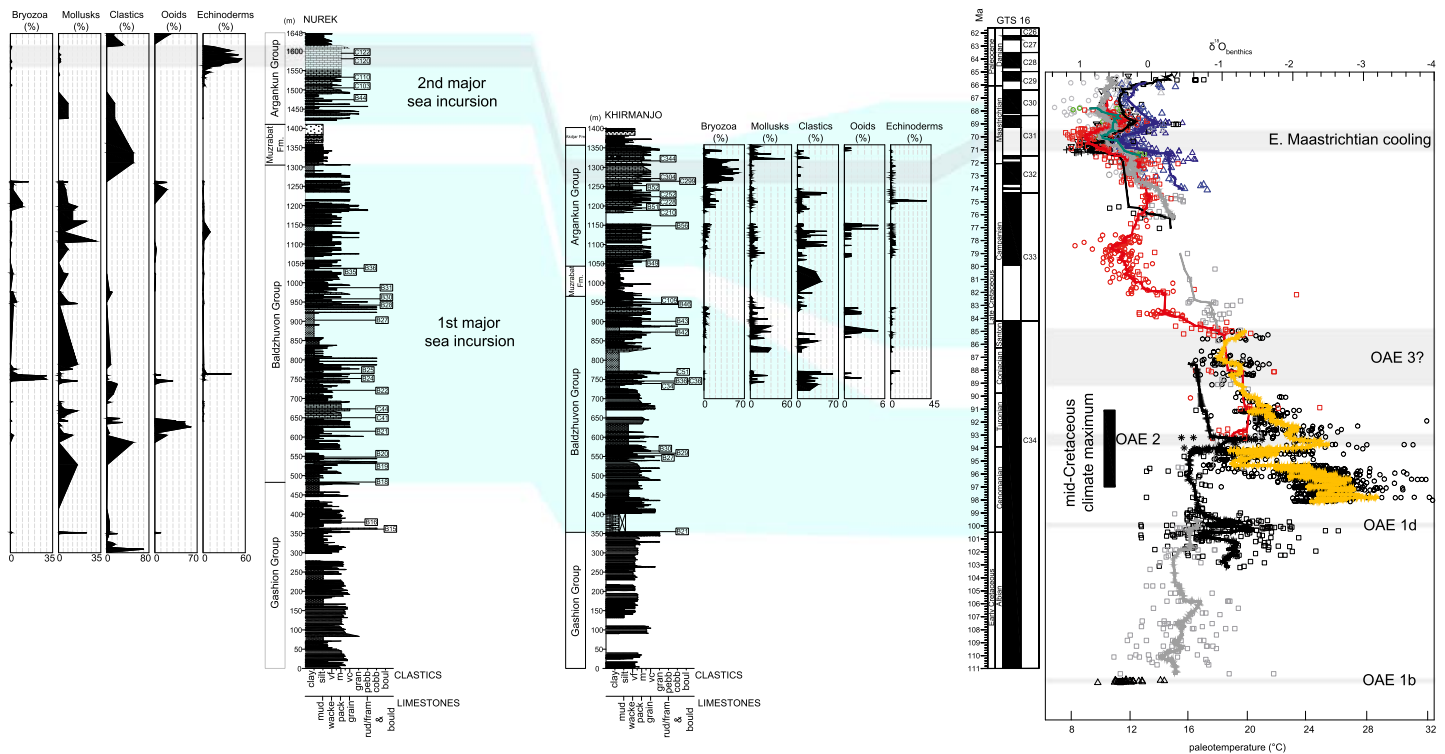
Figure 5. Logs of the Nurek and Khirmanjo sections displaying the changes in the carbonate grain relative abundances (data showing percentages of bioclasts, siliciclastics grains, and ooids). The bryozo- and echinoderm-rich levels (gray shaded areas) at the top of the Nurek and Khirmanjo sections are correlated to the early Maastrichtian cooling event recorded in the compilation of benthic foraminifera stable oxygen isotope data (Friedrich et al., 2012). On this diagram, thick lines show trends through data of different ocean basins (black: North Atlantic; orange: Demerara Rise; gray: southern high latitudes; red: Pacific; blue: subtropical South Atlantic; green: Indian Ocean. OAE = Ocean anoxic event).

based on the analyzed microfossil assemblages. This age constraint is in agreement with several previous studies (Guo et al., 2015; Hao et al., 1982; He, 1991; Pan, 1991; Sobel, 1995; Wang et al., 1990; Yang, 1991; Zhang, 1992) but differs from the previously attributed Cenomanian-Coniacian age by Xi et al. (2016, 2019). With the data present here, the base of the Kukebai Formation is relatively well constrained to the early Cenomanian (ca. 100 Ma), and the age of the top of the Kukebai Formation is less well defined to the early Turonian.

4.5.1.1.3. First Major Regression in the Wuyitake-Muzrabat Formations: Late Turonian-Coniacian (ca. 92?–86 Ma)

The age of the Wuyitake Formation and the time-correlative Muzrabat Formation in the Tajik Basin, corresponding to the first major regression, could be designated as late Turonian-Coniacian based on the constraints from the overlying and underlying Yigeziya (see below) and Kukebai formations. This age estimate is in agreement with the suggested age of He (1991) and Wang et al. (1990), however more difficult to reconcile with the age estimates of Xi et al. (2016, 2019) (Late Coniacian-Early Campanian) and Guo et al. (2015) and Sobel (1995) (Turonian).

4.5.1.1.4. Second Major Sea Incursion in the Yigeziya Formation-Argankun Group: Santonian-Maastrichtian (ca. 86–68? Ma)

The age of the Yigeziya Formation, correlated to the Argankun Group in the Tajik Basin, representing the second major transgression in the Tajik and Tarim basins is constrained to Santonian-Maastrichtian, which is different from the previously suggested ages that range from the Coniacian to Maastrichtian (Chapman et al., 2019; Guo et al., 2015; Pan, 1991; Sobel, 1995; Sun, 1991; Wang et al., 1990; Xi et al., 2016, 2019; Yang, 1991; Zhang, 1992). Based on our age constraint, the onset of the second sea incursion should be during the early Santonian (ca. 86 Ma). The onset of the subsequent regression, however, cannot be further constrained than Maastrichtian.

The Bukhara Formation of Chapman et al. (2019), correlated to the Argankun Group and Yigeziya Formation (Table 1), has previously been assigned a Maastrichtian-Paleogene age. Crucially, these authors also reported the presence of rudist-bearing units near the top of the Bukhara Formation (Sample DSH-16-28, ca. 2,110 m in the Dashtijum section; see their Supplementary Files 4). The rudists observed at the top of the Bukhara Formation cannot be *in situ* if the sediments were indeed deposited after the Cretaceous-Paleogene extinction event. The rudists in the correlative limestone beds in the Khirmanjo section (Figure S2i; see also Dedow et al., 2020) are, however, clearly *in situ*, excluding a Paleogene age for these successions (e.g., Ogg et al., 2016). The base of the Bukhara Formation of Chapman et al. (2019) has been assigned a Maastrichtian age based on the presence of the benthic foraminifera *Omphalocyclus* and *Laffitteina* in Sample DSH16-26 (ca. 1,890 m in Dashtijum section). However, this identification is questionable as the images showing longitudinal sections and details of the forams (Plate 2, figures f–h and i in Supplementary Files 4 of Chapman et al., 2019) appear to lack diagnostic features of *Omphalocyclus* and *Laffitteina*. Specifically, the illustrated specimens lack diagnostic features of *Omphalocyclus*, including a central depression and concave test shape. Normally, *Omphalocyclus* is characterized by a discoidal, centrally depressed biconcave test consisting of a median layer of chamberlets, which doubles and/or then trebles in late ontogenetic stages (Loeblich & Tappan, 1988; Özcan, 2007). Similarly, for *Laffitteina*, the lack of lenticular, planispiral to trochospiral test shape, and other diagnostic features (see Loeblich & Tappan, 1988, for details) does not support this identification. The alternative would be that these microfossils are bryozoan fragments.

4.5.1.1.5. Second Major Regression in the Tuyiluoke-Akdjar Formations: Maastrichtian-Danian

Most of our samples from the Tuyiluoke Formation, correlated to the red gypsiferous mudstone/siltstone unit at the base of the Akdjar Formation in the Tajik Basin, corresponding to the second major regression in the Tajik and Tarim basins were barren or yielded only a few fossils. However, a Maastrichtian-Danian age could be assigned to the Tuyiluoke Formation representing the second major regression based on the foraminiferal assemblages (Guo, 1990; Hao et al., 2001; Hao & Guo, 1990) and the presence of the Cretaceous-Paleogene boundary, identified near the base of the Tuyiluoke Formation in the Tarim Basin (see Kaya et al., 2019, for more discussion; see also Guo, 1990; Tang, Zhong, et al., 1992; Ye et al., 1992).

4.6. Subsidence History

Subsidence curves highly depend on age assignments that are well constrained except for the onset of deposition of the Kezilesu and Gashion clastics during the Early Cretaceous (see section 4.5 above). The poorly constrained onset of deposition may be estimated as old as 145 Ma for the Kezilesu Group in the Tarim Basin and the correlated Gashion Group in the Tajik Basin (e.g., Baratov et al., 1976). However, we show here that the deposition of some part of the Gashion and Kezilesu groups is younger than 126 Ma based on magnetostratigraphy and the onset of deposition may even be younger based on the abovementioned maximum depositional age (99 ± 6 Ma) of Chapman et al. (2019). Considering the oldest and youngest end-member age models, tectonic subsidence increases in the Early Cretaceous until a marked slowdown ca. 92 Ma (Figure 6). In detail, the oldest option, 145 Ma onset of deposition, may also show a slight increase from ca. 100 Ma before the slowdown at ca. 92 Ma (see the curves for the Kezi, Kuzigongsu, 3/34 and 10/43 sections in Figure 6). The youngest option, 99 ± 6 Ma onset of deposition, yields a few million-year timespan for the deposition of the Gashion Group, implying this entire clastic group marks a sudden and drastic increase in tectonic subsidence followed by a slight slowdown at ca. 100 Ma before the marked one at ca. 92 Ma (see the curves for the Nurek and Khirmanjo sections in Figure 6). These detailed changes remain to be established by better age control, but the general regional pattern shows an Early Cretaceous increase in tectonic subsidence followed by a slowdown at ca. 92 Ma.

5. Discussion

5.1. Tectonically Driven Early Cretaceous and First Major Sea Incursions

Our regional compilation indicates a major proto-Paratethys sea incursion into the Tajik foreland basin for the first time during the Early Cretaceous (Aptian, ca. 120 Ma) from the west, shortly after the initiation of the subduction related magmatism (Naidin et al., 1980) (Figure 6). This Early Cretaceous marine incursion corresponds to an increase in tectonic subsidence throughout the basin in the Early Cretaceous (Figure 6). However, the incursion did not reach the eastern Tajik Basin due to the infilling of the basin represented
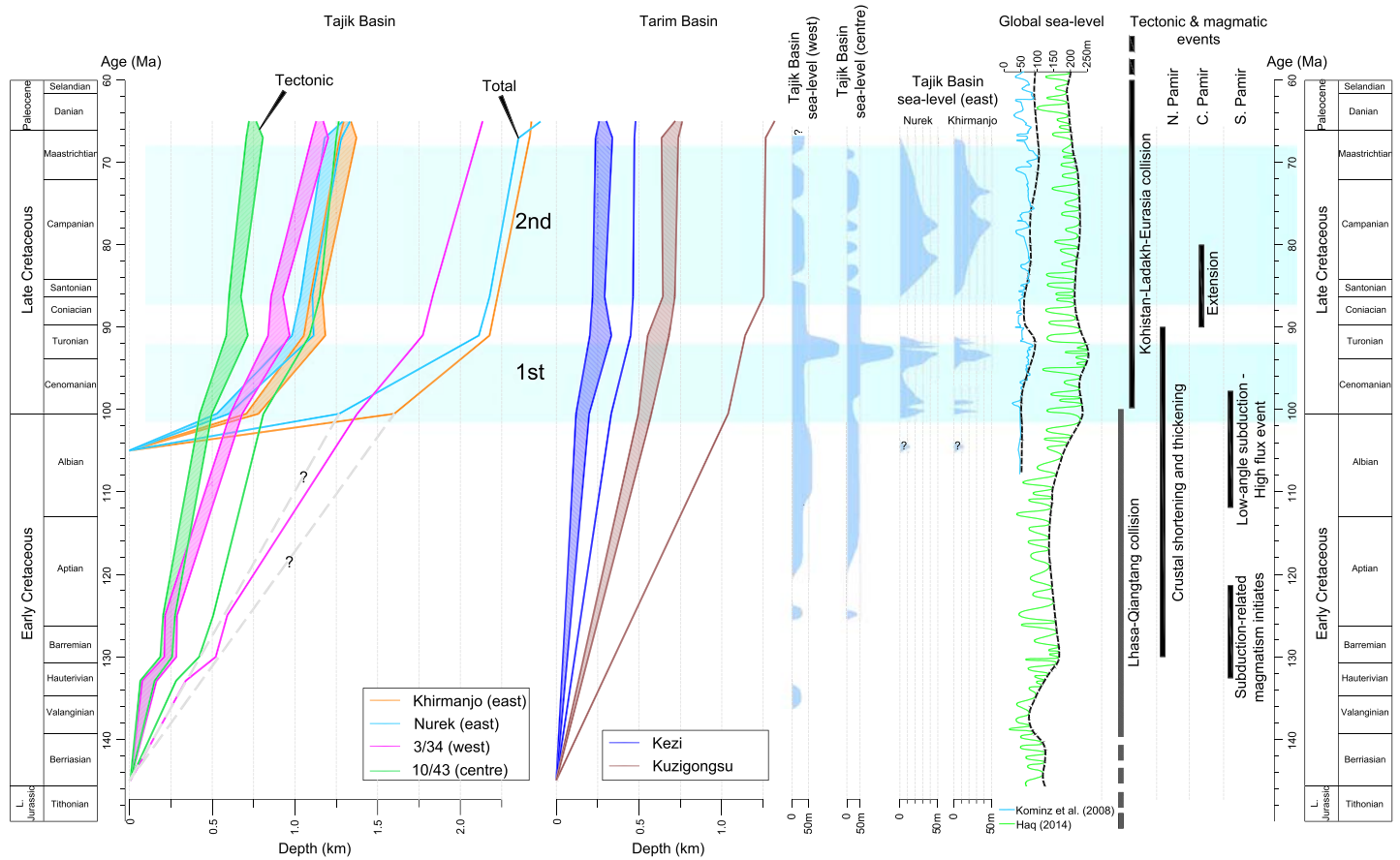
Figure 6. Cretaceous subsidence curves (left) and major sea incursions (cyan shades labeled as first and second) constrained in this study, compared temporally with the Tajik Basin sea level curves, the global sea level curves of Kominz et al. (2008) and Haq (2014) and the regional tectonic and magmatic events (Chapman, Scoggin, et al., 2018). The sea level curves for the west, central, and east Tajik Basin are shown separately; data for the east are from this study, and data for the west and central Tajik Basin are from Naidin et al. (1980).

by the alluvial and coastal plain deposition of the Gashion Group units (Figure 7). During this period, reconstructed global sea level dropped (Figure 6). Considering the very large (several hundred meters) increase in tectonic subsidence in the east and marine incursion during an apparent eustatic lowstand from the west (Figure 6), we argue that tectonism must have been the main driver for the mid-Cretaceous (ca. 120–92 Ma) evolution of the Early Cretaceous and first major sea incursions. However, an eustatic component becomes increasingly likely during the Cenomanian-Turonian hothouse climate, and we argue this climatic factor amplified highstands and enabled the proto-Paratethys Sea to reach its easternmost extent into the Tarim Basin during the first major sea incursion.

The Early Cretaceous tectonic settings of the Tajik and Tarim basins have been previously explored. The Tajik Basin was proposed to be a foreland basin with a Pamir hinterland based on the presence of fragments derived from the clastic rocks in the North Pamir (Zone VI of Burtman & Molnar, 1993). Similarly, the Tarim Basin was also interpreted as a Jurassic-Cretaceous foreland basin based on the occurrence of basin-vergent thrusting during the latest Jurassic (Cobbold et al., 1993; Sobel, 1999). Our results concur with these interpretations. Within the Tajik Basin, the subsidence increases to the southeast, in the sections close to the Pamir, and the lowest subsidence occurs in the central part of the basin. After correction of the Cenozoic counterclockwise rotation (e.g., Thomas et al., 1994), this basin-wide subsidence pattern is consistent with a subsidence in a foreland basin with the foredeep in the southeast, the backbulge in the northwest, and a central forebulge (although we acknowledge that not all foreland basins preserve clear backbulge and forebulge). Similarly, for the southwestern Tarim Basin, published isopach maps for the Cretaceous sedimentary units show a mirrored trend, that is, thicker units close to the Pamir in the southwest and thinner units in the
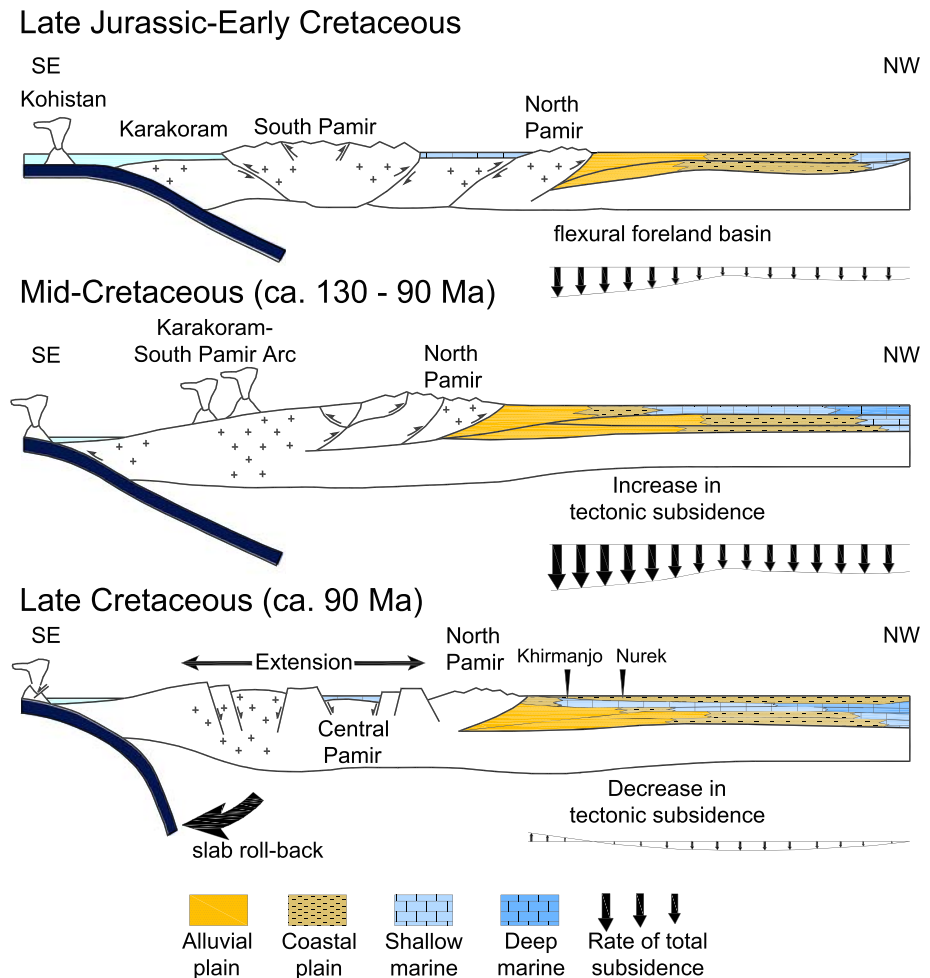
Figure 7. Schematic tectonic evolution of the Pamir and Tajik Basin during the Late Jurassic and Late Cretaceous (modified from Robinson, 2015; Chapman et al., 2019; Chapman, Scoggin, et al., 2018).

center (e.g., Lee, 1985; Sobel, 1995). This pattern suggests that the Tajik and Tarim basins have been the locus of tectonic subsidence associated with crustal thickening in the Pamir since Early Cretaceous time.

To further infer the tectonic setting, we can compare the age of the increase in tectonic subsidence in the Tajik and Tarim basins to reported regional tectonic events in the Pamir. Several studies in the Pamir (e.g., He et al., 2019; Imrecke et al., 2019; Robinson, 2015; Robinson et al., 2004, 2012) provided evidence for Early Cretaceous tectonic deformation. Crustal thickening and shortening in the North Pamir have been evidenced by metamorphic and rapid exhumation events during the mid-Cretaceous (130–100 Ma) by Robinson et al. (2004). During this time, shortening in the North Pamir resulted in north directed thrusting of the Karakul-Mazar terrane over the Kunlun terrane along the northern edge of the Pamir (Robinson et al., 2012). It has also been documented that retro-arc shortening related to Neo-Tethys subduction resulted in the development of the Tanymas-Baoziya-Torbashi thrust as a regionally extensive thrust nappe (He et al., 2019) ca. 120–100 Ma. This regionally extensive thrust nappe development resulted in the imbrication of the Karakul-Mazar and its emplacement on the Central Pamir rocks (Imrecke et al., 2019; Robinson et al., 2012). Robinson et al. (2012) suggested that south directed emplacement of the Karakul-Mazar terrane over the Central Pamir was coeval with Cretaceous shortening to the north. This deformation was also associated to deformation further south in the Karakoram-Hindu Kush, and accordingly, it has been interpreted that a regional compressional event affecting all the Pamir (Robinson, 2015). Furthermore, the U-Pb data from the South Pamir batholith suggest that most subduction-related magmatism occurred between 120 and 90 Ma with a higher volumetric output circa 105 Ma (Aminov et al., 2017; Chapman, Scoggin,

et al., 2018). Similarly, the oldest and youngest ages of the Karakoram batholith have been given as 130 and 95 Ma by Chapman, Scoggin, et al. (2018). Taken together, these data suggest a mid-Cretaceous subduction related, compression-dominated tectonic regime with arc development to the south and retro-arc deformation to the north around 130–90 Ma (Figure 7; Robinson et al., 2012).

The Tajik and Tarim basins are located to the north of the Pamir orogen and, as previously mentioned, have generally been interpreted as retro-arc foreland basins due to the widespread shortening and crustal thickening within the Pamir related to Neo-Tethyan subduction and collisional events along the southern margin of Eurasia (e.g., Chapman, Robinson, et al., 2018, 2019; Hamburger et al., 1992; Hendrix et al., 1992; Robinson, 2015; Sobel, 1999; Şengör, 1979, 1984). These events include the Lhasa-Qiangtang collision leading to the inception of a new subduction zone in the Neo-Tethys (Guilmette et al., 2012) or protracted underthrusting of the Lhasa terrane beneath the Qiangtang block (Kapp et al., 2003) or intrusion of large granitic and granodioritic batholiths onto the southern Pamir (Chapman, Scoggin, et al., 2018). In addition, the collision of the Central Afghan blocks with the south Eurasian margin that occurred during the Late Jurassic-Early Cretaceous may have contributed to the increased tectonic subsidence and controlled the deposition of the Kezilesu and Gashion clastics in the Tarim and Tajik basins, respectively (e.g., Montenat, 2009; Otto, 1997; Tapponnier et al., 1981).

Collectively, we argue that the Early Cretaceous elevated tectonic subsidence is likely due to the crustal thickening and shortening along the northern margin of the Pamir (ca. 130–90 Ma) related to the Lhasa-Qiangtang collision (Robinson et al., 2004) and the collision of the Central Afghan blocks with the south Eurasian margin (e.g., Montenat, 2009; Otto, 1997; Tapponnier et al., 1981). We contend that thrusting along the northern edge of the Pamir at ca. 130–90 Ma resulted in increased subsidence in a retro-arc basin setting and majorly controlled the sea fluctuations during this period.

5.2. Late Cretaceous (>92 Ma) Tectonic Slowdown and Eustatically Driven Second Marine Incursion

Another remarkable result from our subsidence curves is the synchronous slowdown in subsidence at ca. 92 Ma, apparent in all the sections in the Tajik and Tarim basins (Figure 6). At the same time, the maximum thickness of the Late Cretaceous deposits in the central Tajik basin (Burtman, 2000; Chapman et al., 2019) indicates the available accommodation shifted from the southern edge to the center of the basin. This pattern of deposition indicates that the Tajik basin was lacking a forebulge, and a foredeep during this period, suggesting that the deposition took place in an overfilled basin that was already filled by the deposition of Early Cretaceous terrigenous clastic and Cenomanian-Turonian marine strata (e.g., Yang, 2011).

At this time approximately, a shift to lower volume magmatism in the Central Pamir, Karakoram, and within the Kohistan arc has been related to a Neo-Tethyan slab rollback event and associated with extension in the Central Pamir (Burg, 2011; Chapman, Scoggin, et al., 2018; Jagoutz et al., 2007). Along the southern margin of Eurasia, an extensional regime resulting in intra-arc rifting has been explained by a southward rollback of a northward subducting slab beneath the Kohistan arc at ca. 90–80 Ma (Burg, 2011; Burg et al., 2006). During the late Early Cretaceous and Late Cretaceous, a back-arc extension due to a southward rollback of the subducting Neotethys slab controlling the formation of the Xigaze forearc basin and the emplacement of the Gangdese magmatic arc has been also proposed in the southern Tibet (Jolivet, 2017; Zhang et al., 2004). Recently, the rollback of the northward subducting Neo-Tethys slab beneath southern Tibet has been placed to ca. 90 Ma, inducing an upper-plate extension and opening of the Xigaze back-arc basin (Kapp & DeCelles, 2019).

This suggests the ca. 92 Ma slowdown in tectonic subsidence in the Tarim and Tajik basins might relate to a shift from a compressional to an extensional regime in the Central Pamir related to Neo-Tethyan slab rollback. However, the extension does not seem to be expressed in the Tajik and Tarim basins where structures such as normal faults are not observed in that period (e.g., Chapman et al., 2019; Sobel, 1999). It appears the extension affected the Pamir region to the south but not the Tajik and Tarim basins to the north. The slowdown in subsidence is thus rather interpreted here as a decrease in tectonic subsidence during the late orogenic unloading period with limited thrusting (Figure 7). This is reminiscent of the late orogenic unloading period in the foreland basin model of Yang (2011). Following the cessation of intense tectonic activity marked by the slowdown in subsidence, the observed late Turonian-Coniacian regression after the first

major sea incursion may have resulted from increased sediment supply due to continuous erosion of the uplifted thrust belt and rebound of the proximal part of the basin (e.g., Catuneanu, 2004; Yang, 2011). However, no obvious evidence for increased sediment supply or rebound of the proximal part in the studied stratigraphic records has been found. Instead, this major regression coincides with a drop in eustatic sea level curves of Haq (2014) and Kominz et al. (2008) during the late Turonian-Coniacian (Figure 6). Therefore, we interpreted that this major regression is likely related to relative sea level lowering and extensive coastal plain deposition in both basins corresponding to a long-term drop in the global sea level curves of Haq (2014) and Kominz et al. (2008).

We note that the concave up subsidence pattern with slowdown in the Tajik Basin has been previously interpreted as an indicator to an extensional basin in response to lithospheric stretching event followed by slow cooling initiated by the onset of Neo-Tethyan slab rollback (Chapman et al., 2019). However, we find this unlikely because the initial event is rather related to compression in the Early Cretaceous and there is no clear evidence (e.g., normal faults) for a significant extensional event in the Tajik Basin (e.g., Hamburger et al., 1992).

Following the tectonic regime change and relatively low tectonic subsidence during the overfilled period, eustasy appears to play a more dominant role in the proto-Paratethys Sea fluctuations. This is evidenced by the parallel trends of the proto-Paratethys Sea fluctuations with the global sea level reconstructions (Figure 6). Eustatic sea level curves of Haq (2014) and Kominz et al. (2008) indicate a slight increase following the lowstand during the late Turonian-Coniacian, which can also be observed for the proto-Paratethys Sea fluctuations. The fluctuations appear coeval with regional sea fluctuations reported from the West Siberian Basin on the Stable Siberian Platform further supporting a eustatic driving mechanism (Kontorovich et al., 2014) (Figure 8). The second major sea incursion also extended up to the Tarim Basin,
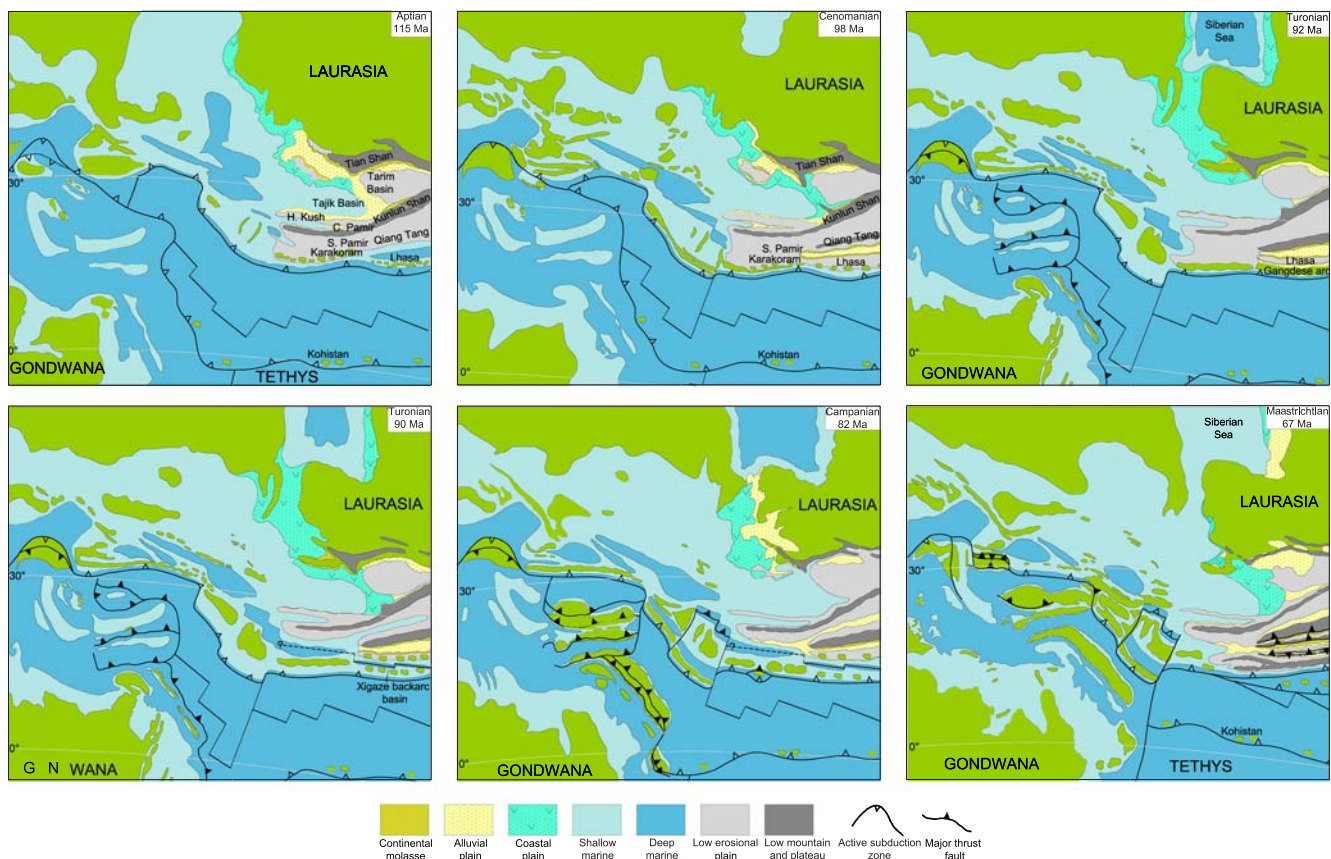
Figure 8. Paleogeographic maps displaying the Cretaceous sea incursions in the Central Asia. Corresponding facies during the transgressions and regressions are indicated.

producing carbonate-dominated epeiric ramp environments until the subsequent regression. Furthermore, the subsequent regression event in the Tajik and Tarim basins appears also coeval with the Maastrichtian regression causing general shallowing and gradual expansion of alluvial and coastal plains in the West Siberian Basin (Kontorovich et al., 2014). Together, these observations strengthen the interpretation that the second sea incursion was mainly driven by eustasy (Figure 8).

5.3. Evidence for Early Maastrichtian Cooling

As mentioned in section 4.4, fossil-bearing carbonate rocks in the Nurek and Khirmanjo sections contain foramol (mollusk and small benthic foraminifera-rich), bryomol (bryozoan-rich), or echinofor (echinoderm-rich) grain association types. Heterozoan bryomol and echinofor grain association types are abundant in nontropical, mostly cool and cold water environments on high-energy open shelves and ramps, whereas foramol type of grain associations are indicative of nontropical, warm temperate environments (Flügel, 2004). Modern-day calcifying reef-building and carbonate platform phototrophs (i.e., corals and larger benthic foraminifera) are found in waters with winter surface temperatures above 20°C, whereas bryozoan-rich heterotrophic communities become dominant in cool waters (<20°C) or in warm settings below the photic zone (Jaramillo-Vogel et al., 2016, and references therein). In terms of trophic conditions, phototrophs, with the exception of red algae, thrive in oligotrophic to slightly mesotrophic conditions while heterotrophs generally dominate in nutrient-rich environments (Jaramillo-Vogel et al., 2016, and references therein).

This temperature-related distribution of heterozoan and photozoan biota might explain the abrupt replacement of mollusks and benthic foraminifera by bryozoan-dominated limestones (bryomol grain association type of Nelson, 1988) at ca. 1,260 m in the Khirmanjo section and by echinoderm-rich limestones at ca. 1,560 m in the Nurek section (Figures 5 and S7). At this level, the proportion of the echinoderm and bryozoan bioclasts rapidly increases up to ca. 60% and dominates the carbonate lithofacies in the Nurek and Khirmanjo sections, respectively. At the top of the Khirmanjo section, ca. 1,325 m, heterozoan bryozoa-rich biota were replaced by photozoan reefal biota (bearing corals, rudists, and red algae), indicating a recovery in the carbonate factory. Species level determination of the bryozoan microfossils could further constrain interpretation of seawater temperature changes through recognition of cool or warm water species (Jaramillo-Vogel et al., 2016; Moissette, 2000). Unfortunately, we were not able to perform taxonomic analysis at the species level on bryozoan microfossils due to their fragmented appearance in thin sections. However, relative percentages of photozoan biota and nonskeletal grains (i.e., ooids, oncoids, and peloids) provide some qualitative constraints regarding the seawater temperatures (Halfar et al., 2004). Halfar et al. (2004) concluded that true cold water heterozoan grain associations contain less than 1% of photozoan components, irrespective of nutrient concentration. In addition, we utilized the presence and abundance of ooid grains, which have been shown preferential occurrence in tropical/warmer climates as a warmer sea water indicator (Flügel, 2004). To adjust for the controlling effect of clastic/nutrient input on the development of grain associations, fluctuations of the clastic content were also evaluated within the Nurek and Khirmanjo sections (Figure 5).

We found that the bryozoan- and echinoderm-rich carbonate beds lack photozoan biota and typical warm water components (i.e., ooids and aggregate grains). One explanation for the absence of photozoan organisms and ooids as well as the outnumbering appearance of the bryozoan and echinoderm beds is a sudden deepening of the environment. However, the deepest environments indicated by the presence of calcisphaerulids are recognized below stratigraphic levels ca. 1,250 m within the Khirmanjo section and ca. 1,510 m within the Nurek section. For a deepening event, an increase in calcisphaerulids would also be expected in the bryozoan- and echinoderm-rich beds, but the bryozoan- and echinoderm-dominated facies do not contain calcisphaerulids or any other evidence (e.g., an increase in planktonic foraminifera) for a deepening event. The input of clastics and associated nutrients decreases both for the Nurek and Khirmanjo sections in the bryozoan- and echinoderm-rich beds, which are mostly pure limestones lacking siliciclastics (Figure 5). Therefore, the terrigenous clastic input had no major effect on the grain association change within the Nurek and Khirmanjo sections. The sheer dominance of heterozoan grain associations and absence of photozoan components strongly suggest that the bryozoan- and echinoderm-rich beds recorded in the Tajik Basin correspond to a cold water heterozoan association. Alternatively, fluctuations in nutrient concentrations could lead to predominance of heterozoan or photozoan associations (Hallock &

Schlager, 1986) and might also have played a role in the formation of the bryozoan- and echinoderm-rich facies in the study area. However, only the clastic input could be evaluated, and the influence of other nutrient sources remains unresolved. Future work revealing nutrient fluctuations, for example, evolution of the total phosphorus (Jaramillo-Vogel et al., 2016), may elucidate the definitive role of nutrients, irrespective of their source.

Intriguingly, the appearance of the heterozoan association coincides with the early Maastrichtian global cooling (ca. 71–70 Ma; Friedrich et al., 2012; Linnert et al., 2014; Miller et al., 1999) (Figure 5). We interpret this as evidence for the Late Cretaceous cooling in Central Asia, which was previously documented in terrestrial settings of eastern China including the Xining-Minhe, Sichuan, Songliao, and Nanxiaong basins (Gao et al., 2015; Li et al., 2018; Ma et al., 2018; Wang et al., 1990, 2013). The observations align well with Maastrichtian climatic fluctuations observed in intermediate and deep waters of different oceanic basins and indicate parallel climatic evolution between deep ocean waters and the sea surface waters of the epicontinental proto-Parathethys Sea.

The final Maastrichtian appearance of photozoan reefal biota at the top of the Khirmanjo section could signal the partial recovery of the carbonate factory, which in turn maybe connected to the late Maastrichtian warming (e.g., Li & Keller, 1998; Linnert et al., 2014; Robinson et al., 2009) (Figure S7). Collectively, shifts in the association types in our studied sections closely follow the global climate trends during the Maastrichtian.

6. Conclusions

Our new age constraints revealed extensive invasion of the proto-Parathethys Sea into the Tajik Basin during the Early Cretaceous (ca. 120 Ma), yet at this time, it did not reach into the Tarim Basin where transitional to nonmarine deposition continued. We related the Early Cretaceous invasion of the sea into the retro-arc Tajik Basin to an increase in tectonic subsidence, caused by thrusting along the northern edge of the Pamir at ca. 130–90 Ma. This thrusting and increased subsidence were linked to coeval compressive deformation in the Pamir related to Neo-Tethyan subduction and collisional events along the southern margin of Eurasia.

The first major sea incursion that did extend into the Tarim Basin occurred during the Cenomanian-Early Turonian (ca. 100–92? Ma). We found this sea incursion was driven mainly by increased subsidence due to tectonics and likely amplified by eustatic highstand, collectively resulting in the maximum geographic extent of the proto-Parathethys Sea during Cretaceous time. The following major regression in the Tajik and Tarim basins occurred during the late Turonian-Coniacian and was likely driven by the eustasy. A regional slowdown in tectonic subsidence at ca. 92 Ma in the Tarim and Tajik basins was found to concur with a shift from a compressional to an extensional regime in the Pamir related to Neo-Tethyan slab rollback. However, the lack of structural evidence (e.g., normal faults) suggests that the extensional event in the Pamir was not expressed in the Tajik and Tarim basins. The slowdown in subsidence was thus rather interpreted here as the cessation of thrusting and tectonic loading during the late orogenic unloading period. Following this change to relatively low tectonic subsidence, eustasy appeared to play a more dominant role in the second major sea incursion (ca. 86–68? Ma) as evidenced by the match with the global sea level reconstructions. A marked lithofacies change in the Tajik Basin from mollusk-rich limestones to bryozoan-rich and echinoderm-rich limestones coincides the global Early Maastrichtian cooling event, suggesting a causal link. Collectively, our integrated data reveal global sea levels and regional tectonic processes alternately controlled the Cretaceous proto-Parathethys Sea incursions in Central Asia.

Data Availability Statement

Data and additional files supporting our analyses and conclusions are in the supporting information and a Mendeley Data repository (https://data.mendeley.com/datasets/6dcxrytc3r/3).

References

Aminov, J., Ding, L., Mamadjonov, Y., Dupont-Nivet, G., Aminov, J., Zhang, L. Y., et al. (2017). Pamir Plateau formation and crustal thickening before the India-Asia collision inferred from dating and petrology of the 110–92 Ma Southern Pamir volcanic sequence. *Gondwana Research*, *51*, 310–326.

Baccelle, L., & Bosellini, A. (1965). Diagrammi per la stima visiva: della composizione percentuale nelle rocce sedimentarie (Vol. 4, No. 3). Università degli studi di Ferrara.

Baratov, R. B., Budanov, V. I., Budanova, K. T., Vlasov, N. G., & Djakov, J. A. (1976). *Subdivisions of stratified and intrusive rocks of Tajikistan* (p. 269). Dushanbe: "Donish" Publishing House. (in Russian)

Barrier, E., Vrielynck, B., Brouillet, J. F., & Brunet, M. F. (2018). *Paleotectonic reconstruction of the Central Tethyan Realm*. Paris, France: Commission for the Geological Map of the World.

Bian, W., Yang, T., Ma, Y., Jin, J., Gao, F., Zhang, S., et al. (2017). New Early Cretaceous palaeomagnetic and geochronological results from the far western Lhasa terrane: Contributions to the Lhasa-Qiangtang collision. *Scientific Reports*, 7(1), 16,216.

Blayney, T., Dupont-Nivet, G., Najman, Y., Proust, J. N., Meijer, N., Roperch, P., et al. (2019). Tectonic evolution of the Pamir recorded in the western Tarim Basin (China): Sedimentologic and magnetostratigraphic analyses of the Aertashi section. *Tectonics*, 38, 492–515. https://doi.org/10.1029/2018TC005146

Blayney, T., Najman, Y., Dupont-Nivet, G., Carter, A., Millar, I., Garzanti, E., et al. (2016). Indentation of the Pamirs with respect to the northern margin of Tibet: Constraints from the Tarim basin sedimentary record. *Tectonics*, 35, 2345–2369. https://doi.org/10.1002/2016TC004222

Borneman, N. L., Hodges, K. V., Soest, M. C., Bohon, W., Wartho, J. A., Cronk, S. S., & Ahmad, T. (2015). Age and structure of the Shyok suture in the Ladakh region of northwestern India: Implications for slip on the Karakoram fault system. *Tectonics*, 34, 2011–2033. https://doi.org/10.1002/2015TC003933

Bosboom, R., Dupont-Nivet, G., Grothe, A., Brinkhuis, H., Villa, G., Mandic, O., et al. (2014). Linking Tarim Basin sea retreat (west China) and Asian aridification in the late Eocene. *Basin Research*, 26(5), 621–640.

Bosboom, R., Mandic, O., Dupont-Nivet, G., Proust, J. N., Ormukov, C., & Aminov, J. (2017). Late Eocene palaeogeography of the proto-Paratethys Sea in Central Asia (NW China, southern Kyrgyzstan and SW Tajikistan). *Geological Society, London, Special Publications*, 427(1), 565–588.

Bouilhol, P., Jagoutz, O., Hanchar, J. M., & Dudas, F. O. (2013). Dating the India-Eurasia collision through arc magmatic records. *Earth and Planetary Science Letters*, 366, 163–175.

Brookfield, M. E., & Hashmat, A. (2001). The geology and petroleum potential of the North Afghan platform and adjacent areas (northern Afghanistan, with parts of southern Turkmenistan, Uzbekistan and Tajikistan). *Earth-Science Reviews*, 55(1–2), 41–71.

Burg, J. P. (2011). The Asia-Kohistan-India collision: Review and discussion. In D. Brown, & P. D. Ryan (Eds.), *Arc-continent collision* (pp. 279–309). Berlin, Heidelberg: Springer.

Burg, J. P., Jagoutz, O., Dawood, H., & Hussain, S. S. (2006). Precollision tilt of crustal blocks in rifted island arcs: Structural evidence from the Kohistan Arc. *Tectonics*, 25, TC5005. https://doi.org/10.1029/2005TC001835

Burnett, J. A. (1998). Upper cretaceous. In P. R. Bown (Ed.), *Calcareous nannofossil biostratigraphy*, *British Micropalaeontology Society Series* (pp. 1–15). London: Chapman and Hall.

Burtman, V. S. (2000). Cenozoic crustal shortening between the Pamir and Tien Shan and a reconstruction of the Pamir-Tien Shan transition zone for the Cretaceous and Palaeogene. *Tectonophysics*, 319(2), 69–92.

Burtman, V. S., & Molnar, P. H. (1993). *Geological and geophysical evidence for deep subduction of continental crust beneath the Pamir* (Vol. 281). America: Geological Society.

Butler, R. F. (1992). *Paleomagnetism: Magnetic domains to geologic terranes* (Vol. 319). Boston, USA: Blackwell Scientific Publications.

Carannante, G., Esteban, M., Milliman, J. D., & Simone, L. (1988). Carbonate lithofacies as paleolatitude indicators: Problems and limitations. *Sedimentary Geology*, 60(1–4), 333–346.

Carrapa, B., DeCelles, P. G., Wang, X., Clementz, M. T., Mancin, N., Stoica, M., et al. (2015). Tectono-climatic implications of Eocene Paratethys regression in the Tajik basin of central Asia. *Earth and Planetary Science Letters*, 424, 168–178.

Catuneanu, O. (2004). Retroarc foreland systems—Evolution through time. *Journal of African Earth Sciences*, 38(3), 225–242.

Chapman, J. B., Carrapa, B., DeCelles, P. G., Worthington, J., Mancin, N., Cobianchi, M., et al. (2019). The Tajik Basin: A composite record of sedimentary basin evolution in response to tectonics in the Pamir. *Basin Research*. https://doi.org/10.1111/bre.12381

Chapman, J. B., Robinson, A. C., Carrapa, B., Villarreal, D., Worthington, J., DeCelles, P. G., et al. (2018). Cretaceous shortening and exhumation history of the South Pamir terrane. *Lithosphere*, 10(4), 494–511.

Chapman, J. B., Scoggin, S. H., Kapp, P., Carrapa, B., Ducea, M. N., Worthington, J., et al. (2018). Mesozoic to Cenozoic magmatic history of the Pamir. *Earth and Planetary Science Letters*, 482, 181–192.

Chen, X., Chen, H., Lin, X., Cheng, X., Yang, R., Ding, W., et al. (2018). Arcuate Pamir in the Paleogene? Insights from a review of stratigraphy and sedimentology of the basin fills in the foreland of NE Chinese Pamir, western Tarim Basin. *Earth-Science Reviews*, 180, 1–16.

Clarke, L. J., & Jenkyns, H. C. (1999). New oxygen isotope evidence for long-term Cretaceous climatic change in the Southern Hemisphere. *Geology*, 27(8), 699–702.

Cobbold, P. R., Davy, P., Gapais, D., Rossello, E. A., Sadybakasov, E., Thomas, J. C., et al. (1993). Sedimentary basins and crustal thickening. *Sedimentary Geology*, 86(1–2), 77–89.

Cowgill, E. (2010). Cenozoic right-slip faulting along the eastern margin of the Pamir salient, northwestern China. *Bulletin of the Geological Society of America*, 122(1–2), 145–161. https://doi.org/10.1130/B26520.1

Dedow, R., Franz, M., Szulc, A., Schneider, J. W., Brückner, J., Ratschbacher, L., et al. (2020). Tajik Basin and southwestern Tian Shan, northwestern India-Asia collision zone: 3. Pre-to syn-orogenic retro-foreland basin evolution in the eastern Tajik depression and linkage to the Pamir Hinterland. *Tectonics*, 39, e2019TC005874. https://doi.org/10.1029/2019TC005874

Dzhalilov, M. R., Alekseev, M. N., Andreev, Y. N., & Salibaev, G. K. (1982). Mesozoic and Cenozoic deposits of the northern part of the Afghano-Tajik Basin. In *Stratigraphic Correlation Between Sedimentary Basins of the ESCAP Region* (Vol. 8, pp. 24–32). New York, USA: UN.

Faisal, S., Larson, K. P., Cottle, J. M., & Lamming, J. (2014). Building the Hindu Kush: Monazite records of terrane accretion, plutonism and the evolution of the Himalaya-Karakoram-Tibet orogen. *Terra Nova*, 26(5), 395–401.

Flügel, E. (2004). *Microfacies of carbonate rocks: Analysis, interpretation and application*. Berlin, Germany: Springer Science & Business Media.

Fraser, J. E., Searle, M. P., Parrish, R. R., & Noble, S. R. (2001). Chronology of deformation, metamorphism, and magmatism in the southern Karakoram Mountains. *Geological Society of America Bulletin*, 113(11), 1443–1455.

Friedrich, O., Norris, R. D., & Erbacher, J. (2012). Evolution of middle to Late Cretaceous oceans—A 55 my record of Earth's temperature and carbon cycle. *Geology*, 40(2), 107–110.

Gao, Y., Ibarra, D. E., Wang, C., Caves, J. K., Chamberlain, C. P., Graham, S. A., & Wu, H. (2015). Mid-latitude terrestrial climate of East Asia linked to global climate in the Late Cretaceous. *Geology*, *43*(4), 287–290.

Gradstein, F. M., Ogg, J. G., Schmitz, M., & Ogg, G. (2012). *The geologic time scale 2012*. Oxford, UK: Elsevier.

Guilmette, C., Hébert, R., Dostal, J., Indares, A., Ullrich, T., Bédard, É., & Wang, C. (2012). Discovery of a dismembered metamorphic sole in the Saga ophiolitic mélange, South Tibet: Assessing an Early Cretaceous disruption of the Neo-Tethyan supra-subduction zone and consequences on basin closing. *Gondwana Research*, *22*(2), 398–414.

Guo, F., Yang, D., Eriksson, K. A., & Guo, L. (2015). Paleoenvironments, stratigraphic evolution and reservoir characteristics of the Upper Cretaceous Yingjisha Group, southwest Tarim Basin. *Marine and Petroleum Geology*, *67*, 336–355.

Guo, R., Li, S., Yu, S., Dai, L., Liu, Y., Peng, Y., et al. (2019). Collisional processes between the Qiangtang Block and the Lhasa Block: Insights from structural analysis of the Bangong-Nujiang Suture Zone, central Tibet. *Geological Journal*, *54*(2), 946–960.

Guo, X. (1990). Study on marine Cretaceous-Tertiary boundary in the western Tarim Basin. *Journal of China University of Geosciences*, *15*, 325–335.

Guo, X. (1991). The depositional environment of the Cretaceous Kizilsu Group in Xinjiang—With a discussion of the lowermost marine horizon of the Cretaceous in the western Tarim Basin. *Acta Geologica Sinica*, *4*, 441–453.

Halfar, J., Godinez-Orta, L., Mutti, M., Valdez-Holguín, J. E., & Borges, J. M. (2004). Nutrient and temperature controls on modern carbonate production: An example from the Gulf of California, Mexico. *Geology*, *32*(3), 213–216.

Hallock, P., & Schlager, W. (1986). Nutrient excess and the demise of coral reefs and carbonate platforms. *PALAIOS*, 389–398.

Hamburger, M. W., Sarewitz, D. R., Pavlis, T. L., & Popandopulo, G. A. (1992). Structural and seismic evidence for intracontinental subduction in the Peter the First Range, central Asia. *Geological Society of America Bulletin*, *104*(4), 397–408.

Hao, Y., & Guo, X. (1990). Cretaceous-Paleocene foraminiferal communities from the western Tarim basin and their environmental significance. *Journal of China University of Geosciences*, *1*, 34–42.

Hao, Y., & Zeng, X. (1984). On the evolution of the west Tarim gulf from Mesozoic to Cenozoic in terms of characteristics of foraminiferal fauna. *Acta Micropalaeotologica Sinica*, *1*, 1–18.

Hao, Y., Zeng, X., & Guo, X. (1988). The marine Cretaceous in the western part of the Tarim Basin of Xinjiang and its depositional environments. *Acta Geologica Sinica*, *1*.

Hao, Y., Zeng, X., & Li, H. (1982). Late Cretaceous and Tertiary strata and foraminifera in western Tarim Basin. Earth Science. *Papers on Paleontology I*, *17*(2), 1–161. (in Chinese)

Hao, Y. C., Guo, X. P., Ye, L. S., Yao, P. Y., Fu, D. R., Li, H. M., & Ruan, P. H. (2001). *The boundary between the marine Cretaceous and Tertiary in the southwest Tarim Basin*. Bejing: Geological Publishing House.

Haq, B. U. (2014). Cretaceous eustasy revisited. *Global and Planetary Change*, *113*, 44–58.

Haq, B. U., Hardenbol, J. A. N., & Vail, P. R. (1987). Chronology of fluctuating sea levels since the Triassic. *Science*, *235*(4793), 1156–1167. https://doi.org/10.1126/science.235.4793.1156

He, C. (1991). Late Cretaceous-Early Tertiary microphytoplankton from the Western Tarim Basin in southern Xinjiang, China. *Najing Institute of Geology and Palaeontology, Academia Sinica*, *235*.

He, J., Kapp, P., Chapman, J. B., DeCelles, P. G., & Carrapa, B. (2019). Structural setting and detrital zircon U-Pb geochronology of Triassic-Cenozoic strata in the eastern Central Pamir, Tajikistan. *Geological Society, London, Special Publications*, *483*(1), 605–630.

Hefu, L. (1986). Geodynamic scenario and structural styles of Mesozoic and Cenozoic basins in China. *AAPG Bulletin*, *70*(4), 377–395.

Hendrix, M. S., Graham, S. A., Carroll, A. R., Sobel, E. R., McKnight, C. L., Schulein, B. J., & Wang, Z. (1992). Sedimentary record and climatic implications of recurrent deformation in the Tian Shan: Evidence from Mesozoic strata of the north Tarim, south Junggar, and Turpan basins, northwest China. *Geological Society of America Bulletin*, *104*(1), 53–79.

Imrecke, D. B., Robinson, A. C., Owen, L. A., Chen, J., Schoenbohm, L. M., Hedrick, K. A., et al. (2019). Mesozoic evolution of the eastern Pamir. *Lithosphere*, *11*(4), 560–580.

Jagoutz, O., Müntener, O., Ulmer, P., Pettke, T., Burg, J. P., Dawood, H., & Hussain, S. (2007). Petrology and mineral chemistry of lower crustal intrusions: The Chilas Complex, Kohistan (NW Pakistan). *Journal of Petrology*, *48*(10), 1895–1953.

Jaramillo-Vogel, D., Bover-Arnal, T., & Strasser, A. (2016). Bryozoan beds in northern Italy as a shallow-water expression of environmental changes during the Oligocene Isotope Event 1. *Sedimentary Geology*, *331*, 148–161.

Jaramillo-Vogel, D., Strasser, A., Frijia, G., & Spezzaferri, S. (2013). Neritic isotope and sedimentary records of the Eocene-Oligocene greenhouse-icehouse transition: The Calcare di Nago Formation (northern Italy) in a global context. *Palaeogeography, Palaeoclimatology, Palaeoecology*, *369*, 361–376.

Jolivet, M. (2017). Mesozoic tectonic and topographic evolution of Central Asia and Tibet: A preliminary synthesis. *Geological Society, London, Special Publications*, *427*(1), 19–55.

Jolivet, M., Heilbronn, G., Robin, C., Barrier, L., Bourquin, S., Guo, Z., et al. (2013). Reconstructing the Late Palaeozoic-Mesozoic topographic evolution of the Chinese Tian Shan: Available data and remaining uncertainties. *Advances in Geosciences*, *37*, 7–18.

Kapp, P., & DeCelles, P. (2019). Mesozoic-Cenozoic geological evolution of the Himalayan-Tibetan orogeny and working tectonic hypotheses. *American Journal of Science*, *319*, 159–254.

Kapp, P., DeCelles, P. G., Gehrels, G. E., Heizler, M., & Ding, L. (2007). Geological records of the Lhasa-Qiangtang and Indo-Asian collisions in the Nima area of central Tibet. *Geological Society of America Bulletin*, *119*(7–8), 917–933.

Kapp, P., Murphy, M. A., Yin, A., Harrison, T. M., Ding, L., & Guo, J. (2003). Mesozoic and Cenozoic tectonic evolution of the Shiquanhe area of western Tibet. *Tectonics*, *22*(4), 1029. https://doi.org/10.1029/2001TC001332

Kaya, M. Y., Dupont-Nivet, G., Proust, J. N., Roperch, P., Bougeois, L., Meijer, N., et al. (2019). Paleogene evolution and demise of the proto-Paratethys Sea in Central Asia (Tarim and Tajik basins): Role of intensified tectonic activity at ca. 41 Ma. *Basin Research*, *31*(3), 461–486.

Khan, S. D., Walker, D. J., Hall, S. A., Burke, K. C., Shah, M. T., & Stockli, L. (2009). Did the Kohistan-Ladakh island arc collide first with India? *Geological Society of America Bulletin*, *121*(3–4), 366–384.

Klocke, M., Voigt, T., Kley, J., Pfeifer, S., Rocktäschel, T., Keil, S., & Gaupp, R. (2017). Cenozoic evolution of the Pamir and Tien Shan mountains reflected in syntectonic deposits of the Tajik Basin. *Geological Society, London, Special Publications*, *427*(1), 523–564.

Kominz, M. A., Browning, J. V., Miller, K. G., Sugarman, P. J., Mizintseva, S., & Scotese, C. R. (2008). Late Cretaceous to Miocene sea-level estimates from the New Jersey and Delaware coastal plain coreholes: An error analysis. *Basin Research*, *20*(2), 211–226.

Kontorovich, A. E., Ershov, S. V., Kazanenkov, V. A., Karogodin, Y. N., Kontorovich, V. A., Lebedeva, N. K., et al. (2014). Cretaceous paleogeography of the West Siberian sedimentary basin. *Russian Geology and Geophysics*, *55*(5–6), 582–609.

Kufner, S. K., Schurr, B., Sippl, C., Yuan, X., Ratschbacher, L., Ischuk, A., et al. (2016). Deep India meets deep Asia: Lithospheric indentation, delamination and break-off under Pamir and Hindu Kush (Central Asia). *Earth and Planetary Science Letters*, *435*, 171–184.

Lan, X., & Wei, J. (1995). *Late Cretaceous-early Tertiary marine bivalve fauna from the western Tarim Basin* (Vol. 212). Beijing: Chinese Science House.

Lebedeva, N. K. (2006). Dinocyst biostratigraphy of the Upper Cretaceous of northern Siberia. *Paleontological Journal*, *40*(5), S604–S621.

Lebedeva, N. K., Aleksandrova, G. N., Shurygin, B. N., Ovechkina, M. N., & Gnibidenko, Z. N. (2013). Paleontological and magnetostratigraphic data on Upper Cretaceous deposits from Borehole No. 8 (Russkaya Polyana District, Southwestern Siberia). *Stratigraphy and Geological Correlation*, *21*(1), 48–78. https://doi.org/10.1134/S086959381301005X

Lee, E. Y., Novotny, J., & Wagreich, M. (2016). BasinVis 1.0: A MATLAB®-based program for sedimentary basin subsidence analysis and visualization. *Computers and Geosciences*, *91*(May), 119–127. https://doi.org/10.1016/j.cageo.2016.03.013

Lee, K. Y. (1985). Geology of the Tarim Basin with special emphasis on petroleum deposits, Xinjiang Uygur Zizhiqu, Northwest Chin. *US Geological Survey Open-File report (No. 85–616)*.

Lees, A., & Buller, A. T. (1972). Modern temperate-water and warm-water shelf carbonate sediments contrasted. *Marine Geology*, *13*(5), M67–M73.

Leith, W. (1985). A mid-Mesozoic extension across Central Asia? *Nature*, *313*(6003), 567.

Li, J., Wen, X., & Huang, C. (2018). Lower and upper Cretaceous paleosols in the western Sichuan Basin, China: Implications for regional paleoclimate. *Geological Journal*, 1–19. https://doi.org/10.1002/gj.3423

Li, L., & Keller, G. (1998). Abrupt deep-sea warming at the end of the Cretaceous. *Geology*, *26*(11), 995–998.

Linnert, C., Robinson, S. A., Lees, J. A., Bown, P. R., Pérez-Rodríguez, I., Petrizzo, M. R., et al. (2014). Evidence for global cooling in the Late Cretaceous. *Nature Communications*, *5*, 4194.

Loeblich, A. R. Jr., & Tappan, H. (1988). *Foraminiferal genera and their classification* (Vol. 2, p. 970). New York: von Nostrand Reinhold Company.

Lukasik, J. J., James, N. P., McGowran, B., & Bone, Y. (2000). An epeiric ramp: Low-energy, cool-water carbonate facies in a Tertiary inland sea, Murray Basin, South Australia. *Sedimentology*, *47*(4), 851–881.

Ma, A., Hu, X., Garzanti, E., Han, Z., & Lai, W. (2017). Sedimentary and tectonic evolution of the southern Qiangtang basin: Implications for the Lhasa-Qiangtang collision timing. *Journal of Geophysical Research: Solid Earth*, *122*, 4790–4813. https://doi.org/10.1002/2017JB014211

Ma, M., Liu, X., & Wang, W. (2018). Palaeoclimate evolution across the Cretaceous-Palaeogene boundary in the Nanxiong Basin (SE China) recorded by red strata and its correlation with marine records. *Climate of the Past*, *14*(3), 287–302.

Mao, S., & Norris, G. (1988). *Late Cretaceous-early Tertiary dinoflagellates and acritarchs from the Kashi area, Tarim Basin, Xinjiang Province, China*. Toronto ON: Royal Ontario Museum Life Sciences Publications.

Miller, K. G., Barrera, E., Olsson, R. K., Sugarman, P. J., & Savin, S. M. (1999). Does ice drive early Maastrichtian eustasy? *Geology*, *27*(9), 783–786.

Miller, K. G., Wright, J. D., & Browning, J. V. (2005). Visions of ice sheets in a greenhouse world. *Marine Geology*, *217*(3–4), 215–231.

Moissette, P. (2000). Changes in bryozoan assemblages and bathymetric variations. Examples from the Messinian of northwest Algeria. *Palaeogeography, Palaeoclimatology, Palaeoecology*, *155*(3–4), 305–326.

Montenat, C. (2009). The Mesozoic of Afghanistan. *GeoArabia*, *14*(1), 147–210.

Naidin, D. P., Sasonova, I. G., Pojarkova, Z. N., Djalilov, M. R., Papulov, G. N., Senkovsky, Y., et al. (1980). Cretaceous transgressions and regressions on the Russian Platform, in Crimea and Central Asia. *Cretaceous Research*, *1*(4), 375–387.

Nelson, C. S. (1988). An introductory perspective on non-tropical shelf carbonates. *Sedimentary Geology*, *60*(1–4), 3–12.

Nikolaev, V. G. (2002). Afghan-Tajik depression: Architecture of sedimentary cover and evolution. *Russian Journal of Earth Sciences*, *4*(6).

Ogg, J. G., Ogg, G., & Gradstein, F. M. (2016). *A concise geologic time scale: 2016*. Amsterdam: Elsevier.

Otto, S. C. (1997). Mesozoic-Cenozoic history of deformation and petroleum systems in sedimentary basins of Central Asia; implications of collisions on the Eurasian margin. *Petroleum Geoscience*, *3*(4), 327–341.

Özcan, E. (2007). Morphometric analysis of the genus Omphalocyclus from the Late Cretaceous of Turkey: New data on its stratigraphic distribution in Mediterranean Tethys and description of two new taxa. *Cretaceous Research*, *28*(4), 621–641.

Pan, H. (1991). *Marine Late Cretaceous –Early Tertiary Gastropod Fossils from Western Tarim Basin* (pp. 1–100). Beijing: Science Press.

Pearce, M. A., Jarvis, I., & Tocher, B. A. (2009). The Cenomanian-Turonian boundary event, OAE2 and palaeoenvironmental change in epicontinental seas: New insights from the dinocyst and geochemical records. *Palaeogeography Palaeoclimatology Palaeoecology*, *280*, 207–234. https://doi.org/10.1016/j.palaeo.2009.06.012

Peyrot, D. (2011). Late Cretaceous (Late Cenomanian-Early Turonian) dinoflagellate cysts from the Castilian Platform, northern Spain. *Palynology*, *35*, 267–300. https://doi.org/10.1080/01916122.2010.523987

Pojarkova, Z. N. (1984). The Cenomanian and Turonian in northeastern Central Asia. *Cretaceous Research*, *5*(1), 1–14.

Pomar, L., Brandano, M., & Westphal, H. (2004). Environmental factors influencing skeletal grain sediment associations: A critical review of Miocene examples from the western Mediterranean. *Sedimentology*, *51*(3), 627–651.

Popov, S. V., Rögl, F., Rozanov, A. Y., Steininger, F. F., Shcherba, I. G., & Kovac, M. (2004). Lithological-paleogeographic maps of Paratethys-10 maps Late Eocene to Pliocene. *Courier Forschungsinstitut Senckenberg*, *250*, 1–42.

Ramstein, G., Fluteau, F., Besse, J., & Joussaume, S. (1997). Effect of orogeny, plate motion and land-sea distribution on Eurasian climate change over the past 30 million years. *Nature*, *386*(6627), 788.

Replumaz, A., Negredo, A. M., Villasenor, A., & Guillot, S. (2010). Indian continental subduction and slab break-off during Tertiary collision. *Terra Nova*, *22*(4), 290–296.

Robertson, A. H., & Collins, A. S. (2002). Shyok Suture Zone, N Pakistan: Late Mesozoic-Tertiary evolution of a critical suture separating the oceanic Ladakh Arc from the Asian continental margin. *Journal of Asian Earth Sciences*, *20*(3), 309–351.

Robinson, A. C. (2015). Mesozoic tectonics of the Gondwanan terranes of the Pamir plateau. *Journal of Asian Earth Sciences*, *102*, 170–179.

Robinson, A. C., Ducea, M., & Lapen, T. J. (2012). Detrital zircon and isotopic constraints on the crustal architecture and tectonic evolution of the northeastern Pamir. *Tectonics*, *31*, TC2016. https://doi.org/10.1029/2011TC003013

Robinson, A. C., Yin, A., Manning, C. E., Harrison, T. M., Zhang, S. H., & Wang, X. F. (2004). Tectonic evolution of the northeastern Pamir: Constraints from the northern portion of the Cenozoic Kongur Shan extensional system, western China. *Geological Society of America Bulletin*, *116*(7–8), 953–973.

Robinson, N., Ravizza, G., Coccioni, R., Peucker-Ehrenbrink, B., & Norris, R. (2009). A high-resolution marine 187Os/188Os record for the late Maastrichtian: Distinguishing the chemical fingerprints of Deccan volcanism and the KP impact event. *Earth and Planetary Science Letters*, *281*(3–4), 159–168.

Rutte, D., Ratschbacher, L., Khan, J., Stübner, K., Hacker, B. R., Stearns, M. A., et al. (2017). Building the Pamir-Tibetan Plateau—Crustal stacking, extensional collapse, and lateral extrusion in the Central Pamir: 2. Timing and rates. *Tectonics*, 36, 385–419. https://doi.org/10.1002/2016TC004294

Rutte, D., Ratschbacher, L., Schneider, S., Stübner, K., Stearns, M. A., Gulzar, M. A., & Hacker, B. R. (2017). Building the Pamir-Tibetan Plateau—Crustal stacking, extensional collapse, and lateral extrusion in the Central Pamir: 1. Geometry and kinematics. *Tectonics*, 36, 342–384. https://doi.org/10.1002/2016TC004293

Schlanger, S. O., & Jenkyns, H. C. (1976). Cretaceous oceanic anoxic events: Causes and consequences. *Geologie en Mijnbouw*, 55(3–4).

Schwab, M., Ratschbacher, L., Siebel, W., McWilliams, M., Minaev, V., Lutkov, V., et al. (2004). Assembly of the Pamirs: Age and origin of magmatic belts from the southern Tien Shan to the southern Pamirs and their relation to Tibet. *Tectonics*, 23, TC4002. https://doi.org/10.1029/2003TC001583

Sclater, J. G., & Christie, P. A. (1980). Continental stretching: An explanation of the post-mid-Cretaceous subsidence of the central North Sea basin. *Journal of Geophysical Research*, 85(B7), 3711–3739.

Şengör, A. M. C. (1979). Mid-Mesozoic closure of Permo-Triassic Tethys and its implications. *Nature*, 279, 590–593.

Şengör, A. M. C. (1984). The Cimmeride orogenic system and the tectonics of Eurasia. *Geological Society of America Special Paper*, 195, 82.

Şengör, A. M. C., Natal'In, B. A., & Burtman, V. S. (1993). Evolution of the Altaid tectonic collage and Palaeozoic crustal growth in Eurasia. *Nature*, 364(6435), 299.

Sissingh, W. (1977). Biostratigraphy of Cretaceous calcareous nannoplankton. *Geologie en Mijnbouw*, 56, 37–65.

Sobel, E. R. (1995). Basin analysis and apatite fission-track thermochronology of the Jurassic-Paleogene southwest Tarim Basin, NW China [Phd dissertation] (p. 308). Stanford, CA: Stanford University.

Sobel, E. R. (1999). Basin analysis of the Jurassic-Lower Cretaceous southwest Tarim basin, northwest China. *Geological Society of America Bulletin*, 111(5), 709–724.

Sobel, E. R., Chen, J., & Heermance, R. V. (2006). Late Oligocene-Early Miocene initiation of shortening in the Southwestern Chinese Tian Shan: Implications for Neogene shortening rate variations. *Earth and Planetary Science Letters*, 247(1–2), 70–81.

Sobel, E. R., Chen, J., Schoenbohm, L. M., Thiede, R., Stockli, D. F., Sudo, M., & Strecker, M. R. (2013). Oceanic-style subduction controls late Cenozoic deformation of the Northern Pamir orogen. *Earth and Planetary Science Letters*, 363, 204–218.

Stübner, K., Ratschbacher, L., Rutte, D., Stanek, K., Minaev, V., Wiesinger, M., & Gloaguen, R. (2013). The giant Shakhdara migmatitic gneiss dome, Pamir, India-Asia collision zone: 1. Geometry and kinematics. *Tectonics*, 32, 948–979. https://doi.org/10.1002/tect.20057

Stübner, K., Ratschbacher, L., Weise, C., Chow, J., Hofmann, J., Khan, J., et al. (2013). The giant Shakhdara migmatitic gneiss dome, Pamir, India-Asia collision zone: 2. Timing of dome formation. *Tectonics*, 32, 1404–1431. https://doi.org/10.1002/tect.20059

Sun, D. (1991). *Late Cretaceous brachiopods from the western Tarim Basin, South Xinjiang, China* (pp. 133–150). Beijing: Science Press.

Sun, G., Hu, X., Xu, Y., & BouDagher-Fadel, M. K. (2019). Discovery of Middle Jurassic trench deposits in the Bangong-Nujiang suture zone: Implications for the timing of Lhasa-Qiangtang initial collision. *Tectonophysics*, 750, 344–358.

Sun, J., Windley, B. F., Zhang, Z., Fu, B., & Li, S. (2016). Diachronous seawater retreat from the southwestern margin of the Tarim Basin in the late Eocene. *Journal of Asian Earth Sciences*, 116, 222–231.

Tang, T., Xue, Y., & Yu, C. (1992). *Characteristics and sedimentary environments of the Late Cretaceous to early Tertiary marine strata in the western Tarim, China*. Beijing: Sci. Press.

Tang, T., Yang, H., Lan, X., Yu, C., Xue, Y., Zhang, Y., et al. (1989). *Marine late Cretaceous and early Tertiary stratigraphy and petroleum geology in Western Tarim Basin, China* (pp. 1–155). Beijing: Sci. Press.

Tang, W., Zhong, X., Guo, C., Yan, Z., & Ye, L. (1992). Abnormal event of carbon stable isotope at the boundary between Cretaceous and Tertiary in Altax section in Xinjiang Autonomous region. *Acta Petrolei Sinica*, 13(2), 209–214.

Tapponnier, P., Mattauer, M., Proust, F., & Cassaigneau, C. (1981). Mesozoic ophiolites, sutures, and arge-scale tectonic movements in Afghanistan. *Earth and Planetary Science Letters*, 52(2), 355–371.

Thomas, J. C., Chauvin, A., Gapais, D., Bazhenov, M. L., Perroud, H., Cobbold, P. R., & Burtman, V. S. (1994). Paleomagnetic evidence for Cenozoic block rotations in the Tadjik depression (Central Asia). *Journal of Geophysical Research*, 99(B8), 15,141–15,160.

Thomas, J. C., Cobbold, P. R., Shein, V. S., & Le Douaran, S. (1999). Sedimentary record of late Paleozoic to recent tectonism in central Asia—Analysis of subsurface data from the Turan and south Kazak domains. *Tectonophysics*, 313(3), 243–263.

Tibert, N. E., Colin, J. P., Leckie, R. M., & Babinot, J. F. (2003). Revision of the ostracode genus Fossocytheridea: Mesozoic ancestral root for the modern eurytopic Cyprideis Jones. *Micropaleontology*, 49(3), 205–230.

Wang, B. D., Wang, L. Q., Chung, S. L., Chen, J. L., Yin, F. G., Liu, H., et al. (2016). Evolution of the Bangong-Nujiang Tethyan ocean: Insights from the geochronology and geochemistry of mafic rocks within ophiolites. *Lithos*, 245, 18–33.

Wang, C., Feng, Z., Zhang, L., Huang, Y., Cao, K., Wang, P., & Zhao, B. (2013). Cretaceous paleogeography and paleoclimate and the setting of SKI borehole sites in Songliao Basin, northeast China. *Palaeogeography, Palaeoclimatology, Palaeoecology*, 385, 17–30.

Wang, D., Sun, X., Zhao, Y., & He, Z. (1990). Palynoflora from Late Cretaceous to Tertiary in some regions of Qinghai and Xinjiang. (The study on the micropaleobotany from Cretaceous-Tertiary of the oil bearing basins in some regions of Qinghai and Xinjiang.) Ministry of Geology and Mineral Resources Institute of Geology, Xinjiang Bureau of Petroleum P. 1–179.

Wang, X., Carrapa, B., Chapman, J. B., Henriquez, S., Wang, M., DeCelles, P. G., et al. (2019). Parathethys last gasp in central Asia and late Oligocene accelerated uplift of the Pamirs. *Geophysical Research Letters*, 46, 11,773–11,781. https://doi.org/10.1029/2019GL084838

Wang, X., Sun, D., Chen, F., Wang, F., Li, B., Popov, S. V., et al. (2014). Cenozoic paleo-environmental evolution of the Pamir-Tien Shan convergence zone. *Journal of Asian Earth Sciences*, 80, 84–100.

Watson, M. P., Hayward, A. B., Parkinson, D. N., & Zhang, Z. M. (1987). Plate tectonic history, basin development and petroleum source rock deposition onshore China. *Marine and Petroleum Geology*, 4(3), 205–225.

Williams, G. L., Brinkhuis, H., Pearce, M. A., Fensome, R. A., & Weegink, J. W. (2004). Southern Ocean and global dinoflagellate cyst events compared: Index events for the Late Cretaceous-Neogene. *Proceeding of the Ocean Drilling Program, Scientific Results*, 1–98.

Williams, G. L., & Bujak, J. P. (1989). Mesozoic and Cenozoic dinoflagellates. In *Plankton Stratigraphy: Volume 2, Radiolaria, Diatoms, Silicoflagellates, Dinoflagellates and Ichthyoliths* (pp. 847–964). Cambridge, UK: Cambridge University Press.

Xi, D., Cao, W., Cheng, Y., Jiang, T., Jia, J., Li, Y., & Wan, X. (2016). Late Cretaceous biostratigraphy and sea-level change in the southwest Tarim Basin. *Palaeogeography Palaeoclimatology Palaeoecology*, 441, 516–527.

Xi, D., Wan, X., Li, G., & Li, G. (2019). Cretaceous integrative stratigraphy and timescale of China. *Science China Earth Sciences*, 62(1), 256–286.

Yang, H., Jiang, X., & Lin, S. (1995). *Late Cretaceous-early Tertiary ostracod fauna from Western Tarim basin, S. Xinjiang, China*. Beijing: Science Press.

Yang, H.-R., Tang, T.-F., Lan, X., Hu, L.-Y., Yu, C.-L., Zhang, Y.-Y., et al. (1983). A preliminary study of the Upper Cretaceous of the Western Tarim Basin (South Xinjiang, China) with special reference to its transgressions. *Zitteliana*, *10*, 115–121.

Yang, S. (1991). *Late Cretaceous and Early Tertiary Echinoids from Tarim Basin* (pp. 101–132). Beijing: Science Press.

Yang, W., Dupont-Nivet, G., Jolivet, M., Guo, Z., Bougeois, L., Bosboom, R., et al. (2015). Magnetostratigraphic record of the early evolution of the southwestern Tian Shan foreland basin (Ulugqat area), interactions with Pamir indentation and India–Asia collision. *Tectonophysics*, *644*, 122–137.

Yang, Y. (2011). Tectonically-driven underfilled-overfilled cycles, the Middle Cretaceous in the northern Cordilleran foreland basin. *Sedimentary Geology*, *233*(1–4), 15–27.

Yang, Z. Y., Wang, Q., Zhang, C., Yang, J. H., Ma, L., Wang, J., et al. (2019). Cretaceous (~ 100 Ma) high-silica granites in the Gajin area, Central Tibet: Petrogenesis and implications for collision between the Lhasa and Qiangtang Terranes. *Lithos*, *324*, 402–417.

Ye, D., Tang, W., Wei, J., Xu, D., & Mao, X. (1992). Geochemical markers of the Cretaceous-Tertiary boundary event in the Altax section. Tarim Basin. *Acta Petrolei Sinica*, *13*(2), 202–208.

Zhang, C. L., Zou, H. B., Li, H. K., & Wang, H. Y. (2013). Tectonic framework and evolution of the Tarim Block in NW China. *Gondwana Research*, *23*(4), 1306–1315.

Zhang, K. J., Xia, B. D., Wang, G. M., Li, Y. T., & Ye, H. F. (2004). Early Cretaceous stratigraphy, depositional environments, sandstone provenance, and tectonic setting of central Tibet, western China. *GSA Bulletin*, *116*(9–10), 1202–1222.

Zhang, S. (1992). Calcareous nannofossils from the Upper Cretaceous and Lower Tertiary in the Western Tarim Basin, South Xinjiang, China. *Xinjiang Stratigraphic Research Series*, *5*, 1–121.

References From the Supporting Information

Boudaugher-Fadel, M. K. (2018). *Evolution and geological significance of larger benthic foraminifera*. London, UK: UCL Press.

Bown, P. R., & Young, J. R. (1998). Introduction. In P. R. Bown (Ed.), *Calcareous nannofossil biostratigraphy*, *British Micropalaeontology Society Series* (pp. 1–15). London: Chapman and Hall.

Bown, P. R., & Young, J. R. (2019). The fossil record of coastal coccolithophores. *Journal of Nannoplankton Research*, *4*, 73–80.

Catuneanu, O. (2006). *Principles of sequence stratigraphy*. Oxford, UK: Elsevier. https://doi.org/10.5860/CHOICE.44-4462

Fensome, R. A., & Williams, G. L. (2004). *The Lentin and Williams index of fossil dinoflagellates 2004 edition* (p. 909). Coll. Station. Tex: Am. Assoc. of Strat.

Fisher, R. A. (1953). Dispersion on a sphere. *Proceedings of the Royal Society of London. Series A: Mathematical and Physical Sciences*, *217*(1130), 295–305.

Gulliford, A. R., Flint, S. S., & Hodgson, D. M. (2017). Crevasse splay processes and deposits in an ancient distributive fluvial system: The lower Beaufort Group, South Africa. *Sedimentary Geology*, *358*, 1–18. https://doi.org/10.1016/j.sedgeo.2017.06.005

Handford, C. R. (1986). Facies and bedding sequences in shelf-storm-deposited carbonates—Fayetteville shale and Pikin limestone (Mississippian), Arkansas. *Journal of Sedimentary Petrology*, *56*(1), 123–137.

Harms, J. C., Southard, J. B., & Walker, R. G. (1982). Structures and sequences in clastic rocks. In *Soc. Econ. Paleontologists and Mineralogists Short Course No. 9*. Tulsa, Oklahoma, USA: SEPM.

Irwin, M. L. (1965). General theory of epeiric clear water sedimentation. *AAPG Bulletin*, *49*(4), 445–459.

Kirschvink, J. L. (1980). The least-square line and plane and the analysis of paleomagnetic data. *Geophysical Journal of the Royal Astronomical Society*, *62*, 699–718.

Lees, J. A., Bown, P. R., & Young, J. R. (2006). Photic zone palaeoenvironments of the Kimmeridge Clay Formation (Upper Jurassic, UK) suggested by calcareous nannoplankton palaeoecology. *Palaeogeography Palaeoclimatology Palaeoecology*, *235*, 110–134.

Perch-Nielsen, K. (1985). Mesozoic Calcareous Nannofossils. In H. M. Bolli, J. B. Saunders, & K. Perrch-Nielsen (Eds.), *Plankton Straitigraphy* (pp. 329–426). Cambridge: Cambridge University Press.

Proust, J. N., Mahieux, G., & Tessier, B. (2001). Field and seismic images of sharp-based shoreface deposits: Implications for sequence stratigraphic analysis. *Journal of Sedimentary Research*, *71*(6), 944–957.

Sibley, D. F., & Gregg, J. M. (1987). Classification of dolomite rock textures. *SEPM Journal of Sedimentary Research*, *57*. https://doi.org/10.1306/212F8CBA-2B24-11D7-8648000102C1865D

Strasser, A. (1986). Ooids in Purbeck limestones (lowermost Cretaceous) of the Swiss and French Jura. *Sedimentology*, *33*(5), 711–727.

Tessier, B. (1993). Upper intertidal rhythmites in the Mont-Saint-Michel Bay (NW France): Perspectives for paleoreconstruction. *Marine Geology*, *110*(3–4), 355–367. https://doi.org/10.1016/0025-3227(93)90093-B

Warren, J. K., & Kendall, C. G. S. C. (1985). Comparison of sequences formed in marine Sabkha (subaerial) and Salina (subaqueous) settings—Modern and ancient. *AAPG Bulletin*, *69*(6), 1013–1023.

Wilson, J. L. (1975). *Carbonate facies in geologic history* (p. 471). Berlin: Springer-Verlag.

Young, J. R., Bown, P. R., & Lees, J. A. (2019). Nannotax3 website. International Nannoplankton association. Accessed 21 Apr. 2019. http://www.mikrotax.org/Nannotax3

Young, J. R., Wade, B. S., & Huber, B. T. (Eds.) (2019). pforams@mikrotax website. Accessed 18 July 2019. URL: http://www.mikrotax.org/pforams